cmgh
CELLULAR AND MOLECULAR GASTROENTEROLOGY AND HEPATOLOGY

ORIGINAL RESEARCH

Loss of MMR and TGFBR2 Increases the Susceptibility to Microbiota-Dependent Inflammation-Associated Colon Cancer

Elena Tosti,[1,*] Ana S. Almeida,[2] Tam T. T. Tran,[3] Mariel Barbachan e Silva,[4] Pilib Ó. Broin,[4] Robert Dubin,[1] Ken Chen,[1] Amanda P. Beck,[5] Andrew S. Mclellan,[6] Eduardo Vilar,[7] Aaron Golden,[4] Paul W. O'Toole,[2] and Winfried Edelmann[1,*]

[1]*Department of Cell Biology, Albert Einstein College of Medicine, Bronx, New York;* [2]*APC Microbiome Ireland and School of Microbiology, University College Cork, Cork, Ireland;* [3]*University of Science and Technology of Hanoi, Vietnam Academy of Science and Technology, Hanoi, Vietnam;* [4]*School of Mathematics, Statistics and Applied Mathematics, National University of Ireland Galway, Galway, Ireland;* [5]*Department of Pathology, Albert Einstein College of Medicine, Bronx, New York;* [6]*Department of Genetics and Genomic Sciences, Mount Sinai School of Medicine, New York, New York; and* [7]*Department of Clinical Cancer Prevention, University of Texas MD Anderson Cancer Center, Houston, Texas*

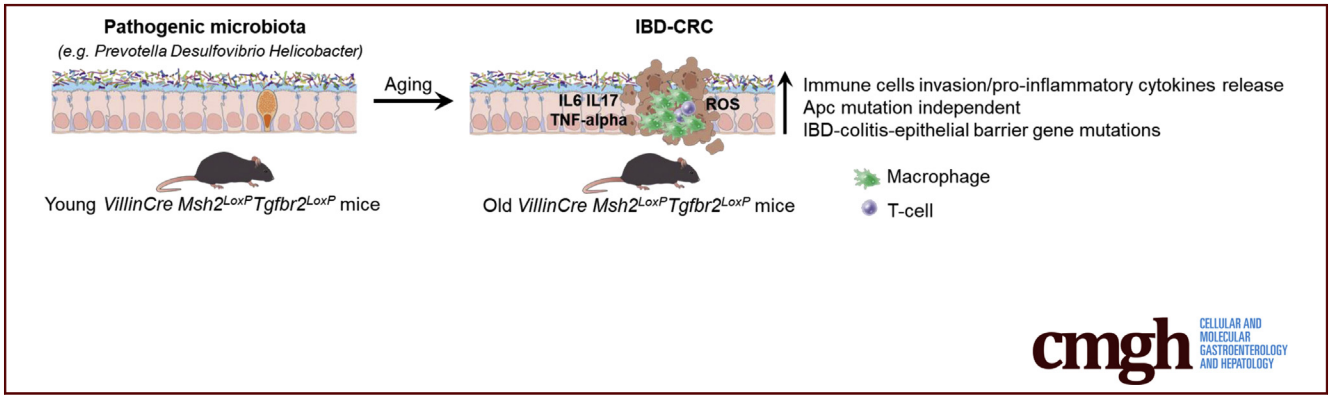

SUMMARY

We present a murine model that demonstrates the synergistic effects of DNA mismatch repair deficiency and the early loss of TGFBR2 in inflammation-associated colon tumorigenesis (inflammatory bowel disease—associated colorectal cancer [IBD-CRC]). Importantly, we found that the mutational and transcriptional alterations in these IBD-CRCs were highly similar to those observed in human IBD-CRCs and highlight the importance of the initial microbiota composition in the development of IBD-CRCs.

BACKGROUND AND AIMS: Mutations in DNA mismatch repair (MMR) genes are causative in Lynch syndrome and a significant proportion of sporadic colorectal cancers (CRCs). MMR-deficient (dMMR) CRCs display increased mutation rates, with mutations frequently accumulating at short repetitive DNA sequences throughout the genome (microsatellite instability). The *TGFBR2* gene is one of the most frequently mutated genes in dMMR CRCs. Therefore, we generated an animal model to study how the loss of both TGFBR2 signaling impacts dMMR-driven intestinal tumorigenesis in vivo and explore the impact of the gut microbiota.

METHODS: We generated *VCMsh2/Tgfbr2* mice in which $Msh2^{loxP}$ and $Tgfbr2^{loxP}$ alleles are inactivated by *Villin*-Cre recombinase in the intestinal epithelium. *VCMsh2/Tgfbr2* mice were analyzed for their rate of intestinal cancer development and for the mutational spectra and gene expression profiles of tumors. In addition, we assessed the impact of chemically induced chronic inflammation and gut microbiota composition on colorectal tumorigenesis.

RESULTS: *VCMsh2/Tgfbr2* mice developed small intestinal adenocarcinomas and CRCs with histopathological features highly similar to CRCs in Lynch syndrome patients. The CRCs in *VCMsh2/Tgfbr2* mice were associated with the presence of colitis and displayed genetic and histological features that resembled inflammation-associated CRCs in human patients. The development of CRCs in *VCMsh2/Tgfbr2* mice was strongly modulated by the gut microbiota composition, which in turn was impacted by the TGFBR2 status of the tumors.

CONCLUSIONS: Our results demonstrate a synergistic interaction between MMR and TGFBR2 inactivation in inflammation-associated colon tumorigenesis and highlight the crucial impact of the gut microbiota on modulating the incidence of inflammation-associated CRCs. *(Cell Mol Gastroenterol Hepatol 2022;14:693–717; https://doi.org/10.1016/j.jcmgh.2022.05.010)*

Keywords: DNA Mismatch Repair; Colon Cancer; Gut Microbiota; Inflammation.

Colorectal cancer (CRC) represents the third-most-common cancer type worldwide and is the second leading cause for cancer-related mortality in the United States. Multiple risk factors contribute to its etiology including genetic predisposition, genotoxic and environmental factors, prolonged exposure to chronic inflammation, and unbalanced diet. Importantly, risk factors for CRC are known to interact with gut microbes.[1–3] The study of the gut microbiota involvement in CRC has generated multiple theories for how single or groups of taxa contribute to CRC development: altered microbial metabolites cause loss of intestinal epithelial barrier function, enhanced access of inflammatory bacteria to epithelial cells, combination of bacterial-driven inflammation, and genotoxic activity lead to mutation and hyperplastic transformation followed by adenocarcinoma.[4]

DNA mismatch repair (MMR) plays a crucial role in maintaining the integrity of the genome by removing misincorporated nucleotides that result from errors in DNA replication and by mediating a DNA damage response after exposure to genotoxic agents.[5] Deficient MMR (dMMR) leads to a 50- to 1000-fold increase in mutation rates and is causative for Lynch syndrome (LS) and 15%–20% of sporadic CRCs.[6] The MMR genes most frequently affected in LS and sporadic CRCs are *MSH2* and *MLH1* and encode key components of MMR complexes involved in coordinating mismatch recognition and excision.

dMMR CRCs are characterized by insertion or deletion mutations at microsatellite DNA sequences, termed microsatellite instability (MSI). In dMMR CRCs, MSI frequently occurs in coding repeat sequences, and these mutations are thought to contribute to dMMR intestinal tumorigenesis.[7] A remarkable example of coding MSI is the disruption of the *TGFBR2* gene at a poly(A) repeat occurring in up to 90% of LS and 70%–80% of sporadic dMMR CRCs.[8] TGFBR2 signaling regulates the differentiation of enterocytes in the crypts or villi, acts in re-establishing intestinal crypt homeostasis upon injury,[8] and plays critical roles in controlling cell proliferation and differentiation.[8] In tumorigenesis, TGFB signaling is complex and mediates pro- and antitumoral activities depending on the concurrent gene mutations in cancer cells and characteristics of the cells infiltrating the tumor microenvironment.[9] The high prevalence of *TGFBR2* mutations in MSI-positive CRCs suggests that TGFBR2 inactivation is an essential event in dMMR-driven tumorigenesis. Indeed, studies in *Tgfbr2* knockout mice showed that TGFBR2 functions as a tumor suppressor when tumorigenesis is initiated genetically by *Apc* or *Pten* deletions, by oncogenic *Kras* activation, or chemically by genotoxic or colitogenic insult.[10–13]

TGFBR2 heterozygous mutations cause Loeys-Dietz syndrome, a rare autosomal dominant disease with an increased risk to inflammatory bowel disease (IBD).[14] Studies of inflammation-associated CRCs (IBD-CRCs) showed MSI in 20%–50% of advanced ulcerative colitis–associated CRCs.[15] Interestingly, MSI-positive IBD-CRCs[15] display a high incidence of *TGFBR2* mutations (50%–76% of cases), which is also observed in early dysplastic lesions.[15–17] Interestingly, loss of *TGF-beta* signaling has been linked to gut microbiota alterations in mice.[18]

Here, we demonstrate that the combined loss of MMR and TGFBR2 tumor suppressor genes in intestinal epithelial cells caused the development of mucinous CRCs with histologic and molecular features highly similar to human IBD-CRCs. The analysis of intestinal microbiota in *VCMsh2/Tgfbr2* mice revealed alterations in their taxonomic composition during IBD-CRC tumorigenesis, delineating interactions between intestinal inflammation and microbial dysbiosis in the development of IBD-CRCs. Overall, our studies indicate a role for both MMR and TGFBR2 signaling in protecting from IBD-CRC consistent with the presence of MMR and TGFBR2 mutations in human IBD-CRCs.[19]

Results

Inactivation of Msh2 *and* Tgfbr2 *in the Intestinal Epithelium Induces Colon Tumorigenesis*

To study how the loss of TGFBR2 affects dMMR intestinal tumorigenesis, we generated *Villin-Cre;Msh2*$^{loxP/loxP}$ (*VCMsh2*) and *Villin-Cre;Msh2*$^{loxP/loxP}$*;Tgfbr2*$^{loxP/loxP}$ mice (*VCMsh2/Tgfbr2*). *VCMsh2/Tgfbr2* mice had a significantly reduced lifespan (median survival 8 months) compared with *VCMsh2* mice (median survival 12 months) (Figure 1*A*). Both mouse lines developed intestinal tumors at very high incidence (Table 1 in Figure 1). A large proportion of the intestinal tumors in *VCMsh2/Tgfbr2* mice were localized to the colon (74.16% [n = 66 of 89]), and in 20.2% (n = 18 of 89) of mice they were co-occurring with tumors in the small intestine (SI) (Table 1 in Figure 1). A subset of *VCMsh2/Tgfbr2* mice (23.6% [n = 21 of 89]) developed only SI tumors. *VCMsh2* mice developed tumors only in the SI (89.3% [n = 25 of 28]). The analysis of age and tumor location revealed that *VCMsh2/Tgfbr2* mice with CRCs died faster (average of 7 months), while *VCMsh2/Tgfbr2* mice developing only SI tumors survived longer (9 months on average). *VCMsh2/Tgfbr2* mice developed SI tumors significantly faster than *VCMsh2* mice, indicating that the loss of TGFBR2 also accelerated dMMR SI tumorigenesis (Figure 1*B*).

The CRC-bearing *VCMsh2/Tgfbr2* mice had a thickened mucosa by inflammation with abundant mucous and feces within the colon lumen. *VCMsh2/Tgfbr2* CRCs did not form intraluminal masses characteristic of SI tumors in *VCMsh2*

*Authors share co-corresponding authorship.

Abbreviations used in this paper: 8-oxoG, 8-oxoguanine; CRC, colorectal cancer; dMMR, deficient DNA mismatch repair; DSS, dextran sulfate sodium; ELISA, enzyme-linked immunosorbent assay; GSEA, gene set enrichment analysis; IBD-CRC, inflammatory bowel disease—associated colorectal cancer; IHC, immunohistochemistry; IL, interleukin; IPA, Ingenuity Pathway Analysis; LS, Lynch syndrome; MMR, mismatch repair; MSI, microsatellite instability; MSS, microsatellite stable; OUT, Operational Taxonomic Unit; qPCR, quantitative polymerase chain reaction; rRNA, ribosomal RNA; SI, small intestine; SPF, specific pathogen–free; TNF-α, tumor necrosis factor α.

Most current article

2352-345X
https://doi.org/10.1016/j.jcmgh.2022.05.010

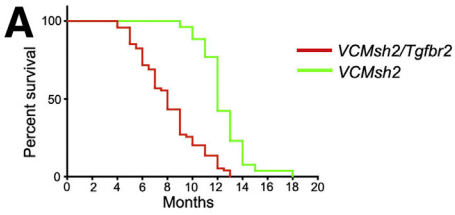

Table 1. Comparison of tumor incidence

Genotype	N	Mice with colon tumor	Mice with SI tumor	Mice with colon + SI tumor	Mice with no tumor
VCMsh2/Tgfbr2	89	48 (53.93%)	21 (23.59%)	18 (20.22%)	2 (2.24%)
VCMsh2	28	0 (0%)	25 (89.3%)	0 (0%)	3 (10.7%)

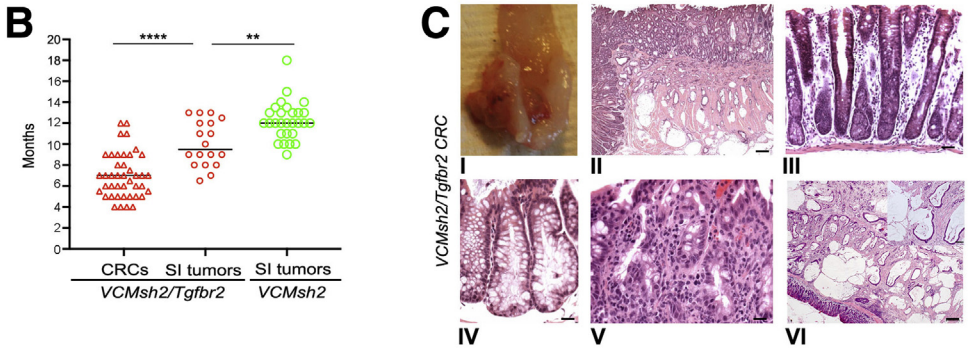

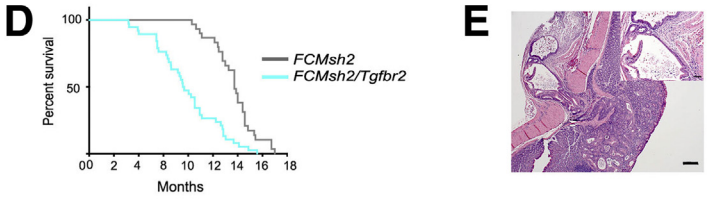

Table 2. Comparison of tumor incidence

Genotype	N	Mice with colon tumor	Mice with SI tumor	Mice with colon + SI tumor	Mice with no tumor	Mice with extra intestinal tumors
FCMsh2/Tgfbr2	38	26 (68.4%)	5 (13.2%)	4 (10.5%)	3 (7.9%)	0 (0%)
FCMsh2	32	0 (0%)	29 (90.6%)	2 (6.3%)	1 (3.1%)	0 (0%)

Figure 1. Inactivation of *Msh2* and *Tgfbr2* in the intestinal epithelium induces colon tumorigenesis. (*A*) Kaplan-Meier analysis. *VCMsh2/Tgfbr2* (n = 89) vs *VCMsh2* (n = 28) $P < .0001$. (*B*) Comparison of tumor occurrence. *VCMsh2/Tgfbr2* CRCs (n = 42; 7 months) vs SI tumors (n = 18; 9.5 months), ****$P < .0001$; *VCMsh2/Tgfbr2* SI tumors (n = 18; 9.5 months) vs *VCMsh2* SI tumors (n = 28, 12 months) **$P = .0019$. (*C*) I, Macroscopic image of *VCMsh2/Tgfbr2* CRC. Representative images: II, hematoxylin and eosin staining of *VCMsh2/Tgfbr2* mucinous CRC (scale bar = 200 μm); III, dysplastic *VCMsh2/Tgfbr2* colon (scale bar = 50 μm); IV, hypertrophy or hyperplasia in goblet cells of *VCMsh2/Tgfbr2* colon mucosa (scale bar = 20 μm); V, colitis in *VCMsh2/Tgfbr2* (scale bar = 20 μm); VI, *VCTgfbr2* mucinous CRC (scale bars = 50 μm, 200 μm). (*D*) Kaplan-Meier analysis. *FCMsh2/Tgfbr2* (n = 38) vs *FCMsh2* (n = 31), ***$P < .0001$. (*E*) *FCMsh2/Tgfbr2* mucinous CRC (scale bars = 50 μm, 200 μm).

mice but were highly invasive, extending through the bowel wall to form large masses on the serosal side (Figure 1*C*-I). Histologically, the CRCs were adenocarcinomas containing large mucin lakes that invaded from the base of the crypts through the lamina propria, submucosa and the muscular layer (Figure 1*C*-II). In *VCMsh2/Tgfbr2* colonic crypts exhibited dysplasia (Figure 1*C*-III) and hypertrophy or hyperplasia of mucosal goblet cells (Figure 1*C*-IV); lymphocytes, plasma cells, and neutrophils expanded the lamina propria and extended multifocally into the underlying submucosa (Figure 1*C*-V). Single mutant *VCTgfbr2* mice were generated during the generation of *VCMsh2/Tgfbr2* mice as well. A small number of *VCTgfbr2* mice developed mucinous CRCs (22.7% [n = 9 of 26]) at an average age of 13 months (Figure 1*B*-VI).

In addition, we generated *Fabp1-Cre; Msh2$^{loxP/loxP}$; Tgfbr2$^{loxP/loxP}$* (*FCMsh2/Tgfbr2*) mice that also displayed reduced survival and developed CRCs, while *Fabp1-Cre/Msh2$^{loxP/loxP}$* (*FCMsh2*) mice developed exclusively SI tumors (Table 2 in Figure 1*D*). Histologically, *FCMsh2/Tgfbr2* CRCs displayed the same mucinous phenotype as the CRCs in *VCMsh2/Tgfbr2* mice (Figure 1*E*). Overall, the increased CRC incidence using 2 different intestine-specific Cre recombinase transgenes indicates a crucial role for TGFBR2 in suppressing dMMR-driven colon tumorigenesis.

Histopathological and Molecular Features of VCMsh2/Tgfbr2 *CRCs*

The intestinal tumors in *VCMsh2/Tgfbr2* mice displayed unique characteristics. The SI tumors differed between genotypes in mucinous content: *VCMsh2/Tgfbr2* mice developed SI adenocarcinomas with extensive mucinous content similar to CRCs (Table 3 in Figure 2*A*-I/II), whereas the SI

Table 3. Mucinous tumor phenotype

Genotype	N	Tumor location	Mucinous phenotype
VCMsh2/Tgfbr2	18	colon	18 (100%)
VCMsh2/Tgfbr2	18	SI	15 (83.3%)
VCMsh2	18	SI	7 (38.8%)

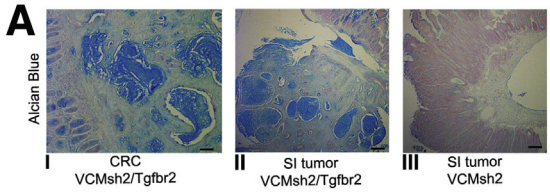

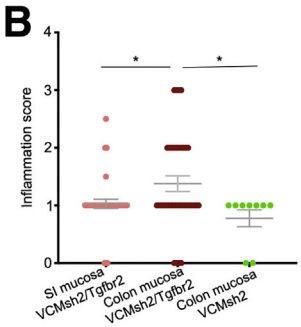

Table 4. Microsatellite analysis of colon tumors

Microsatellite marker	*VCMsh2/Tgfbr2* (n=12)
T27	100% unstable
CA21	90% unstable
TG27	70% unstable

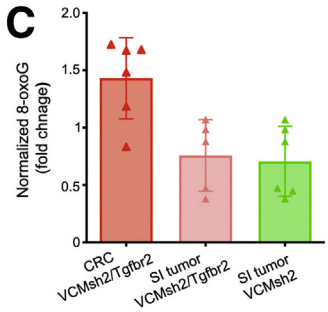

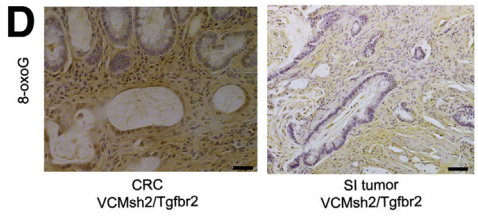

Table 5. Beta-catenin localization

Genotype	N	Tumor location	nuclear beta-catenin
VCMsh2/Tgfbr2	13	colon	0
VCMsh2/Tgfbr2	28	SI	14 (50%)
VCMsh2	20	SI	12 (60%)

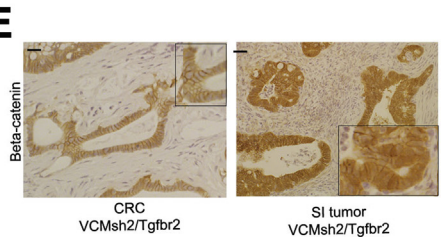

Figure 2. Histologic and molecular features of *VCMsh2/Tgfbr2* intestinal tumors. (*A*) Representative images of Alcian blue staining identifying the blue mucinous lakes: I, *VCMsh2/Tgfbr2* CRC (scale bar = 100 μm); II, *VCMsh2/Tgfbr2* SI tumor (scale bar = 20 μm); III, *VCMsh2* SI tumor (scale bar = 20 μm). (*B*) Inflammation score comparison. *VCMsh2/Tgfbr2* SI (n = 35) vs *VCMsh2/Tgfbr2* colon (n = 37), **P* = .04; *VCMsh2/Tgfbr2* colon vs *VCMsh2* colon (n = 9), **P* = .04. (*C*) 8-oxoG ELISA. *VCMsh2/Tgfbr2* CRCs (n = 6) vs *VCMsh2/Tgfbr2* SI tumors (n = 5), **P* = .03; *VCMsh2/Tgfbr2* CRCs (n = 6) vs *VCMsh2* SI tumors (n = 6), **P* = .015. (*D*) 8-oxoG staining. Increased 8-oxoG nuclear accumulation in *VCMsh2/Tgfbr2* CRCs compared with *VCMsh2/Tgfbr2* SI tumors (scale bar = 50 μm). (*E*) Membrane bound beta-catenin in *VCMsh2/Tgfbr2* CRC and beta-catenin nuclear accumulation in *VCMsh2/Tgfbr2* SI tumor (scale bar = 50 μm).

adenocarcinomas in *VCMsh2* mice displayed mainly villous or tubulovillous growth patterns with minimal to no mucin accumulation (Table 3 in Figure 2*A*-III). The inflammation score in the colonic mucosa and submucosa of *VCMsh2/Tgfbr2* mice was significantly higher compared with their SI tracts and with the colonic mucosa in *VCMsh2* mice (Figure 2*B*). *VCMsh2/Tgfbr2* CRCs displayed high frequency of MSI, as expected (Table 4 in Figure 2). Because MMR facilitates the repair of oxidative DNA damage[20] and inflammation is associated with increased reactive oxygen species production,[21] the loss of MMR and increased inflammation together could result in increased unrepaired oxidative DNA damage. Indeed, enzyme-linked immunosorbent assay (ELISA) and immunohistochemistry (IHC) analyses showed that the genomic DNA in *VCMsh2/Tgfbr2* CRCs contained higher levels of unrepaired 8-oxoguanine (8-oxoG) lesions compared with SI tumors in both *VCMsh2/Tgfbr2* and *VCMsh2* mice (Figure 2*C* and *D*).[3] A canonical feature of colorectal carcinogenesis is dysregulation of WNT signaling, mainly caused by mutation in the *APC* tumor suppressor gene, resulting in the nuclear accumulation of beta-catenin. *VCMsh2/Tgfbr2* CRCs did not show any beta-catenin nuclear localization (Figure 2*E*), whereas SI tumors in both *VCMsh2* and *VCMsh2/Tgfbr2* mice frequently showed widespread beta-catenin nuclear localization (60% and 50%, respectively) (Table 5 in Figure 2*E*).

Mutational Analysis of VCMsh2/Tgfbr2 *Intestinal Tumors*

The histological and molecular differences between SI and colon tumors in *VCMsh2/Tgfbr2* mice suggested that different genetic alterations underlie tumorigenesis in different regions of the intestine. We therefore analyzed the

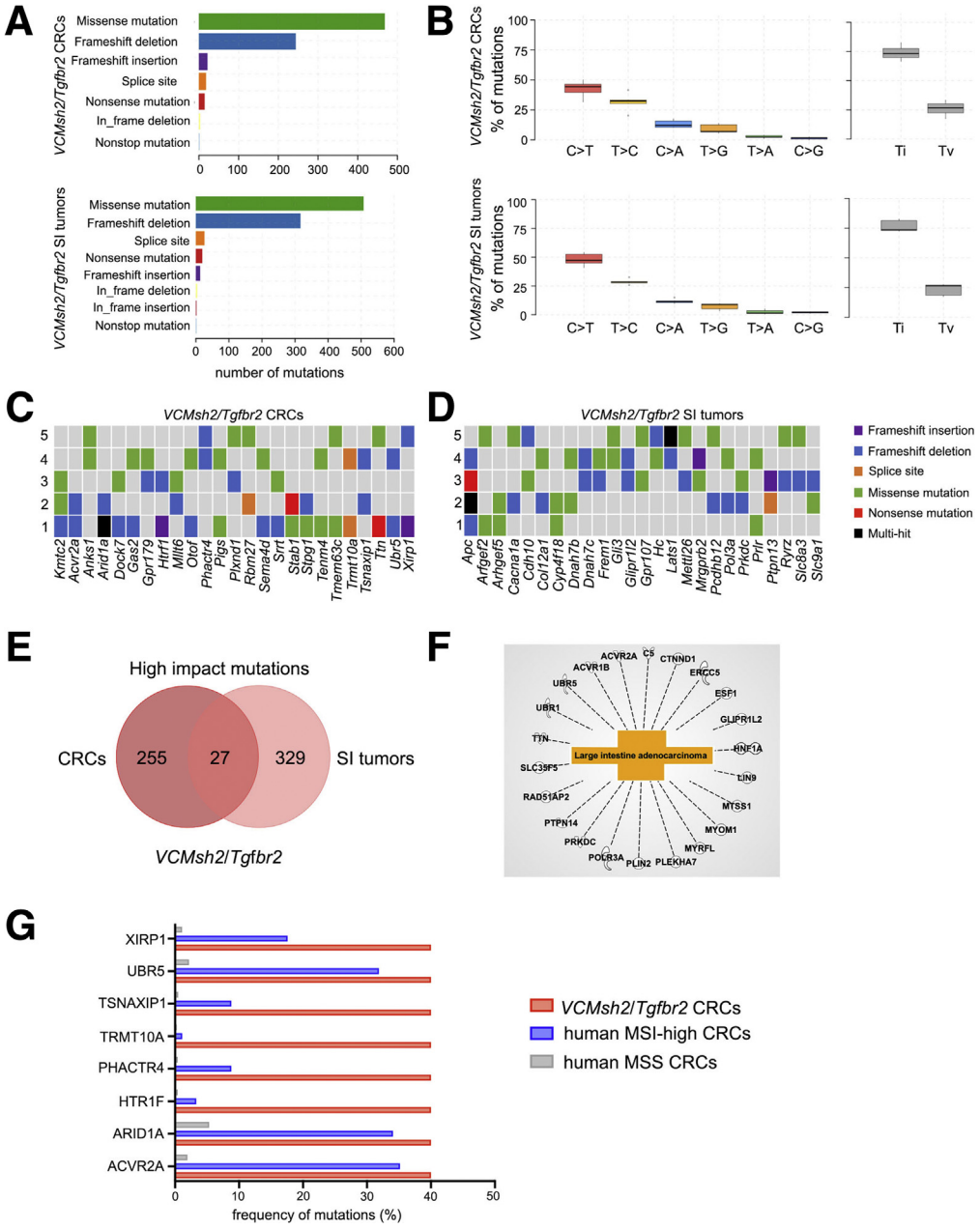

Figure 3. Mutational analysis of *VCMsh2/Tgfbr2* intestinal tumors. (*A*) Number of mutations detected and predicted effect classification in *VCMsh2/Tgfbr2* CRCs (n = 5) and SI tumors (n = 5). (*B*) Distribution of base substitution mutations; frequencies of transversions (Tv) and transitions (Ti). (*C*, *D*) Top 25 genes with a mutation frequency of 40% or higher. (*E*) Venn diagram showing common and unique high-impact-effect mutations between *VCMsh2/Tgfbr2* SI tumors and CRCs. (*F*) IPA analysis of the 27 common high-impact mutations from *E*. (*G*) Mutation frequencies of selected genes; human datasets are originated from cBioPortal datasets.

exome mutational spectra associated with the pathogenesis of SI tumors and CRCs in *VCMsh2/Tgfbr2* mice (n = 5) within the same mouse. In SI tumors we detected an average of 622.8 mutations/tumor (ranging from 514 to 796), CRCs showed an average of 516.6 mutations/tumor (ranging from 201 to 1306). In both SI tumors and CRCs, missense mutations were the most frequent type of alterations, followed by frameshift deletions (Figure 3*A*). The distribution of base changes showed a preponderance of C>T and T>C transitions (Figure 3*B*). The third-most-common type of mutations were C>A transversions, likely resulting from unrepaired oxidative DNA lesions (Figure 3*B*). Overall, the mutational signature resembled that of MSI-positive human tumors consistent with a mutational process caused by dMMR.[22] The variants were annotated and functionally predicted: 374 high- and 503 moderate-impact mutations were present in SI tumors, while 298 high- and 474 moderate-impact variants were found in CRCs.

While these results indicated similarity in the overall variant classification between *VCMsh2/Tgfbr2* SI tumors and CRCs, the analysis of the affected genes revealed significant differences. Consistent with the IHC analyses (Figure 2*E*, Table 5 in Figure 2), the *Apc* gene was mutated in 80% of SI tumors but not in any of the CRCs (Figure 3*C* and *D*). When comparing the genes with high-impact mutations in

Table 6. IPA analysis of "Disease and Disorders"

Disease and Disorders	p-value range	# of molecules
Cancer	1.04E-02 - 3.65E-17	240
Gastrointestinal disease	9.98E-03 - 3.65E-17	229
Organismal Injury and abnormalities	1.08E-02 - 3.65E-17	242

Table 7. IPA analysis of top "Canonical Pathway"

Disease and Disorders	p-value	overlap
Epithelial Adherens Junction Signaling	4.68E-04	5.3% (8/152)
PPARα/RXRα Activation	2.04E-03	4.2% (8/191)
GP6 Signaling Pathway	1.66E-02	4.0% (5/125)

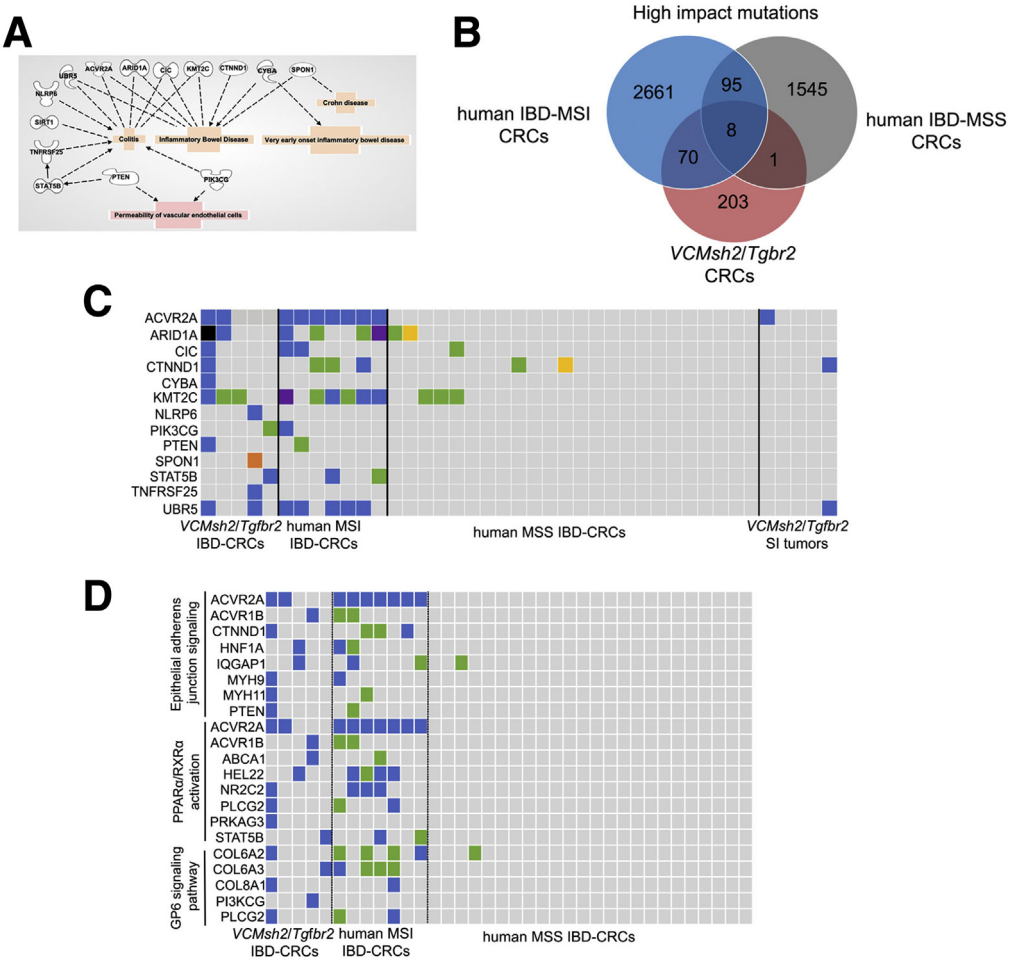

Figure 4. Impact analysis of *VCMsh2/Tgfbr2* mutations in intestinal tumors. (*A*) IPA-generated scheme of mutated genes in *VCMsh2/Tgfbr2* CRCs and their involvement in IBD-associated diseases. (*B*) Venn diagram between predicted high-impact mutations from *VCMsh2/Tgfbr2* CRCs and human IBD-MSI or MSS CRCs. (*C*) List of genes previously found mutated in human IBD-CRCs and colitis that are frequently mutated in both *VCMsh2/Tgfbr2* CRCs and human MSI IBD-CRCs but only rarely in MSS IBD-CRCs and *VCMsh2/Tgfbr2* SI tumors. Each column represents 1 sample: *VCMsh2/Tgfbr2* CRCs/SI tumors, n = 5; human MSI IBD-CRCs, n = 7; human MSS IBD-CRCs, n = 24. The box colors indicate the predicted mutational effect as in the Figure 3*C* and *D* color legend. (*D*) Mutations distribution among human and mouse CRCs datasets among the 3 major top canonical pathways highlighted by IPA analysis.

VCMsh2/Tgfbr2 SI tumors and CRCs, only 27 were in common, all reported to be involved in intestinal tumorigenesis (Figure 3*E* and *F*).

We next analyzed the mutational targets in *VCMsh2/Tgfbr2* CRCs for similarities with human MSI-positive CRCs extracted from the cBioPortal database.[23,24] High-impact mutations occurred recurrently in several genes (*Xirp1*, *Ubr5*, *Tsnaxip1*, *Trmt10a*, *Phactr4*, *Htr1f*, *Arid1a*, *Acvr2*a) that are also mutated at higher frequencies in human MSI-positive CRCs (91 samples) compared with microsatellite stable (MSS) CRCs (1501 samples) (Figure 3*G*).

Core Ingenuity Pathway Analysis (IPA)[25] was employed to investigate the biological functions of genes with high impact mutations in *VCMsh2/Tgfbr2* CRCs. The major disease and functions identified were cancer and gastrointestinal disease (Table 6 in Figure 4). When investigating the top canonical pathways category, *VCMsh2/Tgfbr2* CRC high-impact mutations were enriched in genes belonging to the epithelial adherens junction signaling, PPARα/RXRα activation, and GP6 signaling pathway categories (Table 7 in Figure 4). In addition, IPA Bio-profile analysis identified a group of mutated genes that were previously found associated with colitis or IBD-CRC either in patients or in mouse models (Figure 4*A*).

Finally, we investigated similarities with the available exome data from human IBD-CRCs using a dataset of

high- or moderate-impact mutations from 7 MSI-positive IBD-CRCs and 24 MSS IBD-CRCs.[26] *VCMsh2/Tgfbr2* CRCs shared a higher number of mutations with MSI-positive IBD-CRCs compared with MSS IBD-CRCs (Figure 4*B*). The genes in *VCMsh2/Tgfbr2* CRCs that IPA Bio-profile analysis reported to be involved in colitis or IBD-CRC were also mutational targets predominantly in the human MSI IBD-CRCs (Figure 4*C*). We also observed a marked enrichment in mutations in genes belonging to the 3 top canonical pathways in *VCMsh2/Tgfbr2* CRCs in human MSI IBD-CRCs but not in MSS IBD-CRCs (Figure 4*D*).

The Tumor Microenvironment in VCMsh2/Tgfbr2 *CRCs Is Characterized by an Inflammation-Specific Gene Expression Signature*

To study the impact of the mutational changes on gene expression during *VCMsh2/Tgfbr2* colorectal tumorigenesis, we performed gene expression profiling comparing CRCs with matched tumor-free colonic mucosa (n = 7). A multidimensional scaling plot showed a clear separation of tumor and colonic mucosa samples (Figure 5*A*). Gene set enrichment analysis (GSEA) revealed significant similarities with chronic inflammation signatures in the human colonic

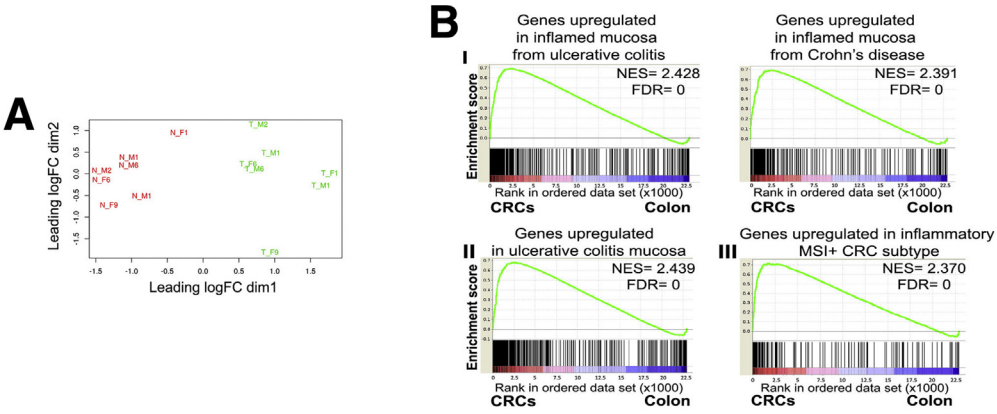

Figure 5. The tumor microenvironment in *VCMsh2/Tgfbr2* CRCs is characterized by an inflammation-specific gene expression signature. (*A*) Multidimensional scaling plot showing clear separation between *VCMsh2/Tgfbr2* CRCs (green) and matched tumor-free mucosa (red). (*B*) GSEA of *VCMsh2/Tgfbr2* CRCs vs matched tumor-free colon mucosa, comparison with multiple signatures. (*C*) Ratio of CD45+/Epcam+ cells in *VCMsh2/Tgfbr2* CRCs (n = 11) vs colon mucosa (n = 11), ***$P < .0001$. (*D*) Representative images of staining for different immune cells: macrophages (F4/80 antibody), T cells (CD3 antibody), and B cells (B220 antibody) in *VCMsh2/Tgfbr2* colon tumor-free mucosa and CRC (scale bars = 200 μm, 50 μm, 20 μm). FDR, false discovery rate; NES, normalized enrichment score.

Table 8. IPA analysis of "Disease and Disorders"

Disease and Disorders	p-value range	# of molecules
Inflammatory response	9.18E12-3.08E-52	467
Endocrine system disorders	2.42E12-8.83E-46	243
Gastrointestinal disease	2.61E12-8.83E-46	385
Metabolic disease	1.08E12-8.83E-46	300
Organismal Injury and abnormalities	1.60E11-8.83E-46	996

Table 9. IPA analysis of "Diseases or Functions annotations"

Disease and Disorders	p-value range	Activation z-score	# of molecules
Cell movment of phagocytes	3.08E-52	6.298	160
Activation of leukocytes	1.17E-36	3.555	153
Cell movement of neutrophils	5.43E-34	4.138	92
Immune response of cells	5.24E-27	4.096	124
Cell movement of macrophages	1.95E-21	3.243	69
Recruitment of macrophages	2.0E-17	3.435	36
Transmigration of phagocytes	6.18E-16	3.072	29
Activation of macrophages	7.22E-22	3.934	51

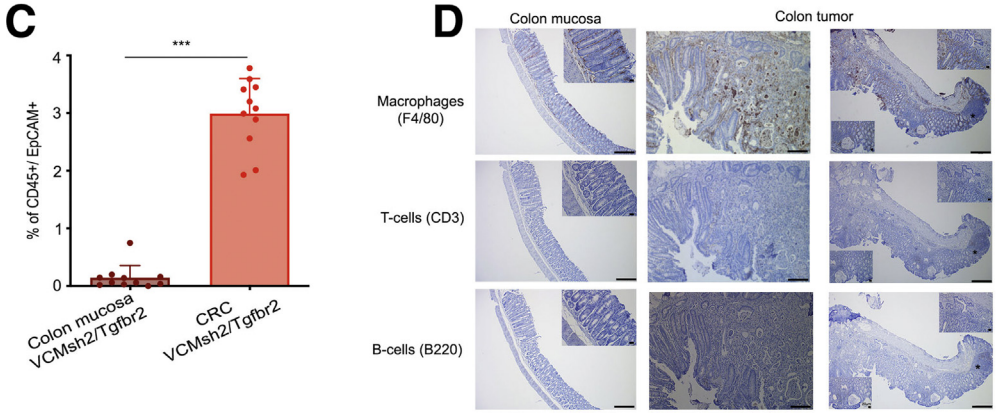

mucosa (Figure 5*B*-I, II)[27] as well as in human MSI-positive inflammatory-CRCs (Figure 5*B*-III).[28] IPA yielded a list of genes within the disease and disorders category that were significantly overrepresented in *VCMsh2/Tgfbr2* CRCs, including genes in pathways involved in inflammatory response and gastrointestinal and metabolic disease (Table 8 in Figure 5). IPA disease and function annotations within the inflammatory response disease category predicted increased recruitment and activity of distinct immune cell types within the *VCMsh2/Tgfbr2* CRC microenvironment (Table 9 in Figure 5). Consistent with this, CD45+ cells were significantly enriched within the tumor microenvironment compared with matched colonic mucosa (Figure 5*C*). We observed significant macrophage infiltration throughout CRC tissues and increased focal T cell infiltration, whereas B cell presence was limited to the lymphoid tissue associated with the colon tumors (Figure 5*D*). Upstream regulator IPA further predicted increased activation of proinflammatory cytokines that act as tumor growth and survival factors in human IBD-CRCs including interleukin (IL)-6, tumor necrosis factor α (TNF-α), and IL-17A (Table 10 in Figure 6).[21] Their overexpression was confirmed by quantitative polymerase chain reaction (qPCR) (Figure 6*A*). TNF-α expression was elevated in tumor-free mucosa and significantly increased in tumors. TNF-α staining was particularly widespread in the colonic mucosa compared with SI mucosa in *VCMsh2/Tgfbr2* mice (Figure 6*B*-I, III). A similarly increased TNF-α staining was

Table 10. IPA analysis of TNF-alpha , IL6 and IL17

Upstream regulator	Predicted activation state	Activation z-score	p-value of overlap
TNF-alpha	activated	7.117	7.29E-70
IL6	activated	5.692	3.07E-29
IL17A	activated	3.89	1.02E-14

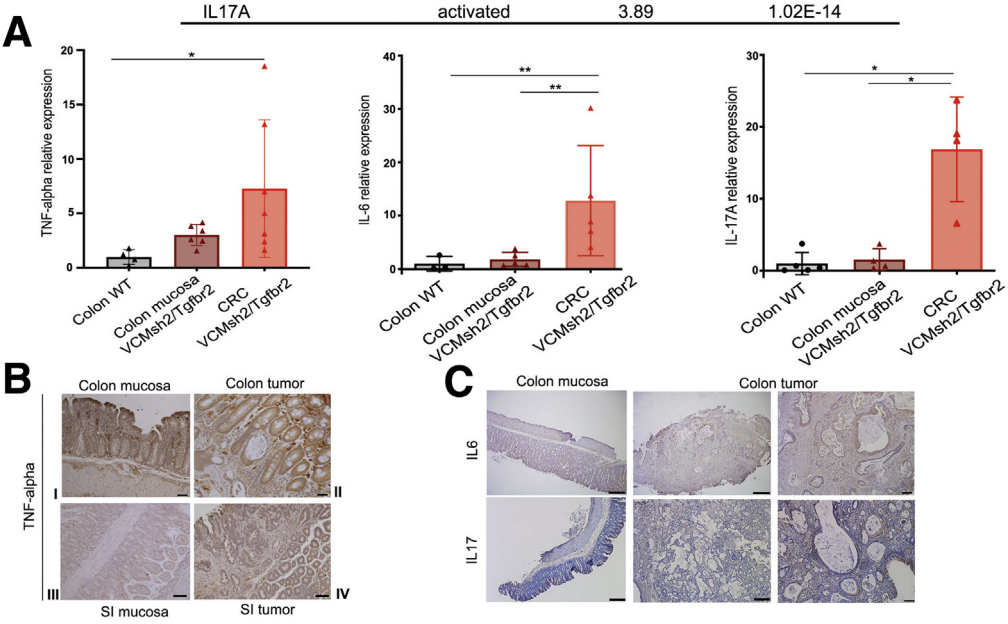

Table 11. IPA analysis of upstream regulators

Upstream regulator	Predicted activation state	Activation z-score	p-value of overlap	Relevance from literature
LPS (Lipopolysaccharide)	activated	7.159	3.18E-78	inflammation
NF-kB (complex)	activated	5.339	1.36E-19	inflammation
STAT3	activated	4.739	1.47E-22	inflammation
NOS2 (iNOS)	activated	2.029	0.00000267	inflammation
HNF1A	inhibited	-3.145	0.00000133	mutated in human CRCs
SPDEF	inhibited	-3.675	5.58E-07	lost in human CRCs

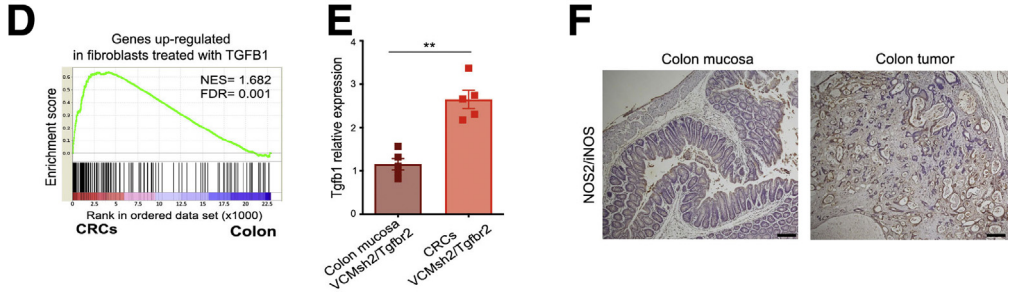

Figure 6. Characterization of inflammatory factors in the *VCMsh2/Tgfbr2* CRCs tumor microenvironment. (*A*) qPCR. TNF-α: wild-type (WT) vs *VCMsh2/Tgfbr2* CRCs colon (n = 7), **P* = .01. IL-6: WT (n = 3) vs *VCMsh2/Tgfbr2* CRCs (n = 5), **P* = .036; *VCMsh2/Tgfbr2* CRCs vs *VCMsh2/Tgfbr2* colon (n = 5), ***P* = .0079. IL-17A WT (n = 5) vs *VCMsh2/Tgfbr2* CRCs (n = 4), **P* = .015; *VCMsh2/Tgfbr2* CRCs vs *VCMsh2/Tgfbr2* colon (n = 4), **P* = .028. (*B*) Representative images of TNF-α staining: I, *VCMsh2/Tgfbr2* colon tumor-free mucosa; II, *VCMsh2/Tgfbr2* CRC (scale bar = 20 μm); III, *VCMsh2/Tgfbr2* SI tumor-free mucosa; IV, SI tumor (scale bar = 50 μm). (*C*) Representative images of staining for IL-6 and IL-17 comparing *VCMsh2/Tgfbr2* colon tumor-free mucosa and tumor (scale bars = 200 μm, 50 μm). (*D*) GSEA of *VCMsh2/Tgfbr2* CRCs vs matched colon mucosa with a signature indicative of TGFB1-treated fibroblast. (*E*) qPCR. *Tgfb1*, CRCs fold change relative to tumor-free colon (n = 5), ***P* = .0079. (*F*) iNOS staining comparing *VCMsh2/Tgfbr2* colon mucosa and CRC in *VCMsh2/Tgfbr2* CRCs (scale bar = 200 μm).

evident when comparing CRCs with SI tumors (Figure 6*B*-II, VI). The increased expression of IL-6 and IL-17 in *VCMsh2/Tgfbr2* CRCs was also confirmed by IHC analyses (Figure 6*C*). A list of gene expression changes predicted to be associated with immune cell infiltration in *VCMsh2/Tgfbr2* CRCs is shown in Supplementary Excel File S6.

IPA upstream regulator analysis in *VCMsh2/Tgfbr2* CRCs also predicted an activated state for some genes involved in inflammation or inhibition of genes lost in human CRCs (Table 11 in Figure 6). The *VCMsh2/Tgfbr2* CRC microenvironment also shared significant similarities with the gene expression signature of human fibroblasts exposed to TGFB1 and its increased expression was verified by qPCR (Figure 6*D* and *E*). iNOS/NOS2 was found widely expressed in *VCMsh2/Tgfbr2* CRC tissue, as predicted by the IPA activation analysis, consistent with an inflammatory CRC environment (Figure 6*F*).

To investigate specifically epithelial CRC cells, we performed additional transcriptomic analyses of sorted epithelial cells to exclude extensive infiltrating immune cells. GSEA highlighted similarities between the gene expression profiles in *VCMsh2/Tgfbr2* CRC epithelial cells and transcriptional signatures derived from human cancer cell lines with PTEN knockdown or oncogenic KRAS overexpression (Figure 7*A*). IPA further showed a significant enrichment in molecules within the disease and disorders category belonging to cancer and gastrointestinal diseases (Table 12 in Figure 7). Several genes with altered expression profiles have also been reported in human CRC and IBD or mouse models of colitis (Table 13 in Figure 7).[29,30,31–36]

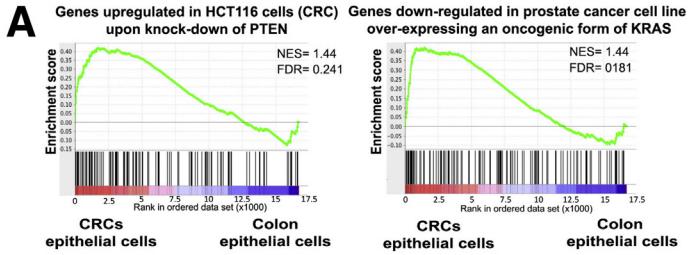

Table 12. IPA analysis of "Disease and Disorders"_CRC epithelial expression profile

Disease and Disorders	p-value range	# of molecules
Cancer	1.18E-02 - 8.48.08E-06	24
Development disorder	1.17E-02 - 8.48.08E-06	14
Gastrointestinal disease	1.17E-02 - 8.48.08E-06	24
Organismal Injury and abnormalities	1.17E-02 - 8.48.08E-06	38

Table 13. Relevant factors in CRC epithelial expression profile

Gene name	change in expression	Relevanance from literature
CLU (Clusterin)	up-regulated	CLU has been proposed as a marker for CRC development associated with poor outcome/decreased disease-free survival
MSLN (Mesothelin)	up-regulated	MSLN has been proposed as a new target for immunotherapy in human solid tumors
CDX2 (Caudal-type homeobox transcription factor 2	down-regulated	CDX2 acts as a tumor suppressor gene in murine and human intestinal cancer/prposed as prognostic biomarker in CRC
CFTR (Cystic fibrosis transmembrane receptor)	down-regulated	CFTR is a tumor suppressor gene in murine and human intestinal cancer
SLC4A4 (Solute carrier family 4 member 4)	down-regulated	SLC4A4 has been reported to be down-regulated in human ulcerative colits patients
SULT1A1 (Sulfotransferase family 1A, member 1)	down-regulated	SULT1A1 has been reported to be down-regulated in human ulcerative colits patients and in murine models of colitis
AQP1 (Aquaporin 1)	down-regulated	Multiple aquaporin isoforms are reported to be reduced in expression in IBD patients and murine models of colitis
CLDN15 (Claudin 15)	down-regulated	CLDN15 modulated Na+ permeability, it is found to be decreased in expression in human CRCs
NLRP6 (NLR family, pyrin domain containing 6)	down-regulated	NLRP6 protects against colitis and colitis-associated carcinogenesis, regulates colonic microbial ecology

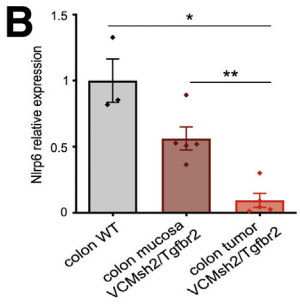

Figure 7. Epithelial tumor cells expression profile analysis of *VCMsh2/Tgfbr2* CRCs. (*A*) GSEA of sorted epithelial cells from *VCMsh2/Tgfbr2* CRCs and matched tumor-free colon mucosa. (*B*) qPCR. Nlrp6: WT (n = 3) vs *VCMsh2/Tgfbr2* CRCs (n = 5), **P* = .035; *VCMsh2/Tgfbr2* colon (n = 5) vs *VCMsh2/Tgfbr2* CRCs (n = 5), ***P* = .0079.

Nlrp6 was of particular interest due to its roles in IBD-CRC and colonic microbial regulation.[37] Indeed, we found *Nlrp6* mutated in a *VCMsh2/Tgfbr2* CRC (Figure 4*C*) and also generally downregulated in *VCMsh2/Tgfbr2* CRCs, which was confirmed by qPCR (Figure 7*B*).

Microbiota Composition Modulates the Susceptibility of VCMsh2/Tgfbr2 *Mice to IBD-CRC*

To study the impact of the microbiota on the susceptibility to IBD-CRCs, *VCMsh2/Tgfbr2* mice were rederived into specific pathogen–free (SPF) recipients and aged in an SPF environment. *VCMsh2/Tgfbr2-SPF* mice had a significantly longer median survival (12 months) compared with *VCMsh2/Tgfbr2* mice in the conventional barrier (8 months) (Figure 8*A*). The SPF environment significantly affected tumor distribution: while 38% (n = 19 of 50) of SPF mice developed CRCs (compared with 74.15% of conventional mice) (Table 14 in Figure 8), a larger proportion developed SI adenocarcinomas (60% [n = 30 of 50]) compared with conventionally aged mice (23.6% [n = 21 of 89]). The colonic mucosa in CRC bearing *VCMsh2/Tgfbr2-SPF* mice displayed lower inflammation (Figure 8*B*) and expressed significantly less TNF-α, indicating a reduced ongoing proinflammatory state (Figure 8*C*). *VCMsh2/Tgfbr2-SPF* mice that developed only SI tumors displayed the lowest inflammation. These results suggested that the intestinal

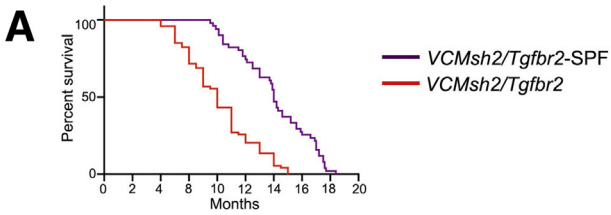

Table 14. Comparison of tumor incidence

Genotype	N	Mice with colon tumor	Mice with SI tumor	Mice with colon + SI tumor	Mice with no tumor
VCMsh2/Tgfbr2	89	48 (53.93%)	21 (23.59%)	18 (20.22%)	2 (2.24%)
VCMsh2/Tgfbr2-SPF	50	11 (22%)	30 (60%)	8 (16%)	1 (2%)

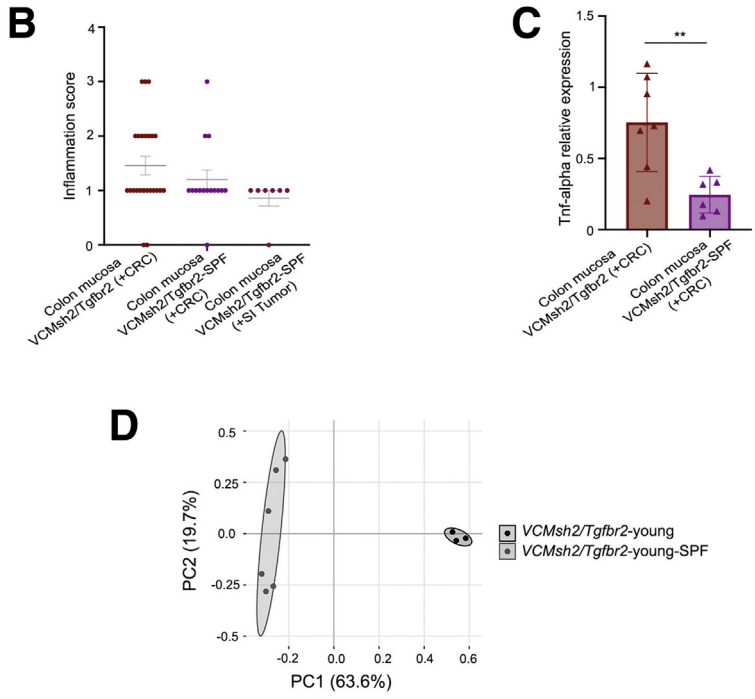

Figure 8. Microbiota composition modulates the susceptibility of *VCMsh2/Tgfbr2* mice to IBD-CRC. (*A*) Kaplan-Meier analysis. *VCMsh2/Tgfbr2* mice (n = 89) vs *VCMsh2/Tgfbr2-SPF* mice aged in the SPF barrier (n = 50), $P < .0001$. (*B*) Inflammation score. *VCMsh2/Tgfbr2* mice with CRC (n = 24), *VCMsh2/Tgfbr2-SPF* mice with CRC (n = 15), *VCMsh2/Tgfbr2-SPF* mice with SI tumors (n = 7); no significant differences. (*C*) qPCR. TNF-α: *VCMsh2/Tgfbr2* (n = 7) vs *VCMsh2/Tgfbr2-SPF* colon (n = 6), $^{**}P = .008$. (*D*) Relatedness (β-diversity) of fecal microbiota composition between the 2 different cohorts of young *VCMsh2/Tgfbr2* mice (n = 3 conventional mice and n = 6 SPF mice). Principal coordinate (PC) analysis plot on Bray-Curtis distance matrix shows a clear separation between the 2 barriers (analyses of similarities test, R=1, $P = .014$).

Table 15. Beta- diversity metrics

ANOSIM test	Unweighted UniFrac		Weighted UniFrac		Bray-Curtis	
	R	*P*	R	*P*	R	*P*
Barrier effect: SPF vs Conventional young	1	.006	0.56	.03	1	.014

microbiota in *VCMsh2/Tgfbr2* mice modulate the severity of colonic inflammation and susceptibility to CRC.

Therefore, we compared the microbiota from conventional barrier and SPF mice at 3 months of age (young and young-SPF, respectively) to determine the initial microbiota composition associated with either the increased or reduced IBD-CRC development by sequencing the 16S ribosomal RNA (rRNA) amplicon in fecal DNA. Differences in global microbiota relatedness were investigated by β-diversity analysis using multiple dissimilarity metrics (Table 15 in Figure 8), which showed clear separation of the *VCMsh2/Tgfbr2* microbiota in the 2 barriers (Figure 8*D*). In young mice, major taxonomic differences specific to each barrier microbiota showed unique distributions between the 2 major phyla: while microbiota in conventional barrier mice were highly enriched in *Bacteroides* and reduced in *Firmicutes*, in SPF mice, the ratio of *Bacteroides* over *Firmicutes* was significantly reduced (Figure 9*A* and 9*B*). Specifically, at the genus level, conventional barrier microbiota contained higher relative proportions of

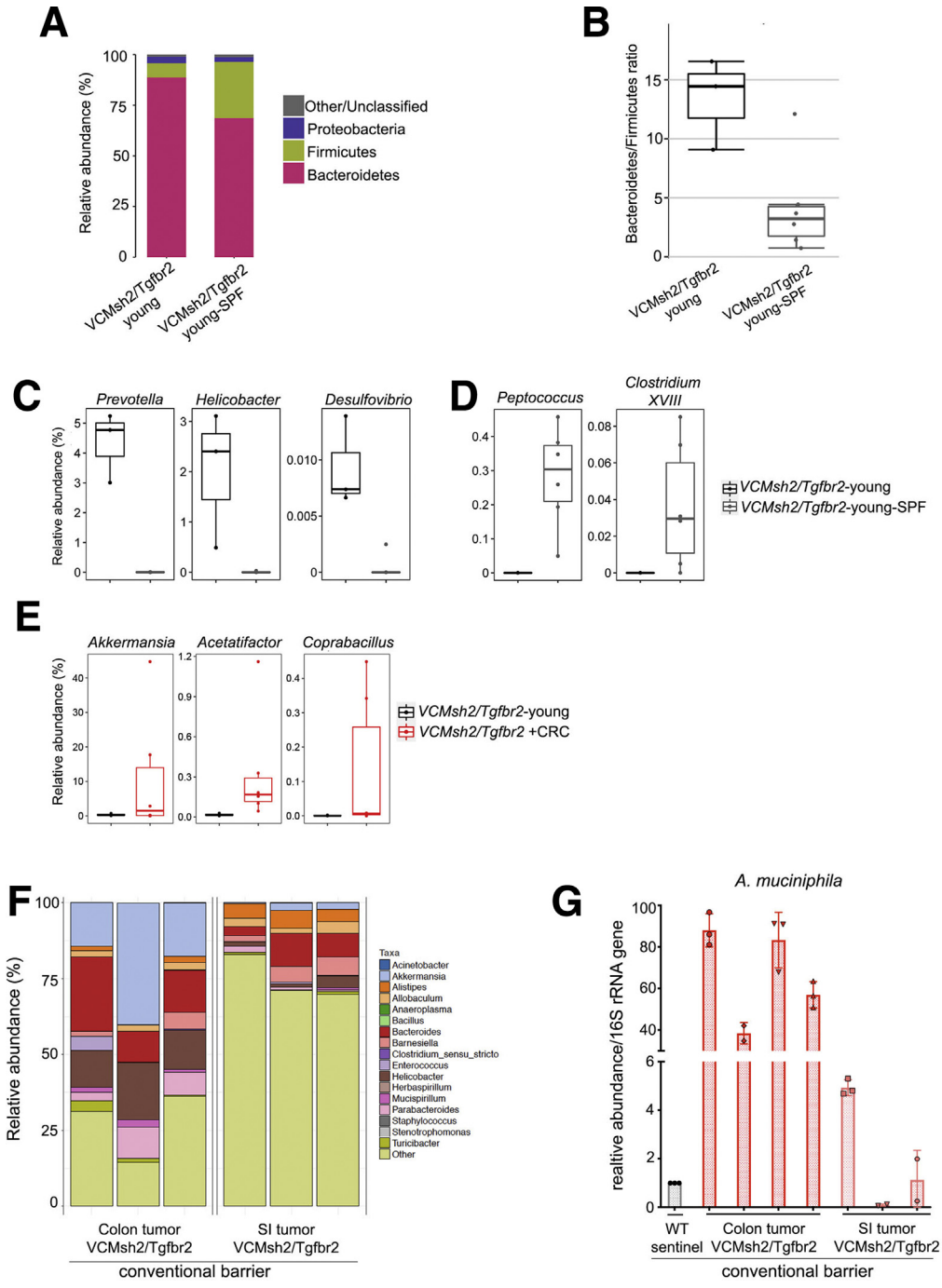

Figure 9. Microbiota changes associated with *VCMsh2/Tgfbr2* IBD-CRC. (*A*) Phyla relative abundance of young mice from the conventional and SPF barriers at 3 months of age. (*B*) Ratio of *Bacteroides/Firmicutes* phyla between young conventional and SPF mice: $P = .048$ (Mann-Whitney *U* test). (*C*, *D*) Box plots of relative abundance, young age comparison between barriers: *Prevotella*, $P = 7.02E\text{-}16$; *Helicobacter*, $P = 2.22E\text{-}12$; *Desulfovibrio*, $P = .006$; *Peptococcus*, $P = 7.29E\text{-}08$; *Clostridium XVIII*, $P = 0.006$. (*E*) Bar plots of the genera significantly increased in *VCMsh2/Tgfbr2* mice with CRCs: *Akkermansia*, $P = .0036$; *Acetatifactor*, $P = .0017$; *Coprobacillus*, $P = .0036$. (*F*) Taxonomic distribution at the genus level from conventional *VCMsh2/Tgfbr2* mice with either SI tumors or CRCs (n = 3); *Akkermansia*, $P = .05$. (*G*) Relative abundance of *A. muciniphila* in conventional *VCMsh2/Tgfbr2* mice with CRCs (n = 4) vs *VCMsh2/Tgfbr2* mice with SI tumors (n = 3). Each column represents a mouse with replicates, the normalized *A. muciniphila* 16S rRNA level is expressed as relative ratio to the sentinel mice, $^{****}P < 001$.

Prevotella, *Helicobacter*, and *Desulfovibrio*, while the SPF microbiota had barely detectable levels of these pathogenic genera (Figure 9*C*). In contrast, no measurable levels of Operational Taxonomic Units (OTUs) for other bacteria such as *Peptococcus* and *Clostridium XVIII* were found in conventional barrier microbiota compared with SPF microbiota (Figure 9*D*).

We then analyzed the microbiota associated with spontaneous IBD-CRC development in conventional barrier mice and observed a marked increase in *Verrucomicrobia*. Three genera were significantly more abundant in conventional barrier *VCMsh2/Tgfbr2* mice carrying inflammation-associated CRCs: *Akkermansia*, *Coprobacillus*, and *Acetatifactor* (Figure 9*E*). These genera were previously found associated with human and mouse CRCs.[38–40] Interestingly, *Akkermansia* did not show any significant expansion in *VCMsh2/Tgfbr2* mice that developed only SI tumors, but it was significantly more abundant in *VCMsh2/Tgfbr2* mice with IBD-CRCs (Figure 9*F* and *G*).

TGFBR2 Status and Microbiota Composition Affect Dextran Sulfate Sodium–Induced Colonic Inflammation and dMMR Colorectal Tumorigenesis

To assess the effects that either the TGFBR2 status or microbiota composition has on dMMR IBD-CRC development in a procolitogenic environment, *VCMsh2, VCMsh2/Tgfbr2*, and *VCMsh2/Tgfbr2-SPF* mice were exposed to DSS. The dextran sulfate sodium (DSS) treatment induced a 100% (n = 20 of 20) penetrant CRC phenotype in *VCMsh2/Tgfbr2* mice with a median survival of 6 months (Figure 10*A*). In contrast, both the presence of TGFBR2 or the SPF environment had a protective effect against DSS-induced colorectal tumorigenesis, with *VCMsh2* and *VCMsh2/Tgfbr2-SPF* mice displaying median survival of 9.3 and 13 months, respectively (Figure 10*A*). The increased survival was associated with reduced CRC incidence: 56.25% (n = 9 of 16) of *VCMsh2* mice and 53.3% (n = 8 of 15) of *VCMsh2/Tgfbr2-SPF* mice developed DSS-induced CRCs (Table 16 in Figure 10). While TGFBR2 expression in *VCMsh2* mice caused only a moderate reduction in DSS-induced inflammation compared with *VCMsh2/Tgfbr2* mice, a significant reduction was seen in *VCMsh2/Tgfbr2-SPF* mice (Figure 10*B*). Furthermore, *VCMsh2* mice rapidly gained weight upon cessation of DSS treatment, while *VCMsh2/Tgfbr2* mice recovered at a significantly slower rate (Figure 10*C*). Tumor incidence analysis performed at early time points after cessation of DSS treatment showed that *VCMsh2/Tgfbr2* mice had already developed CRCs during treatment (4 CRCs in 5 mice at 12 days; 6 CRCs in 5 mice at 30 days). In contrast, in *VCMsh2* mice, only 1 adenoma was found at 12 days (1 in 3 mice) and none at 30 days post–DSS treatment (0 in 4 mice) (Table 17 in Figure 11).

The DSS-induced CRCs in *VCMsh2* and *VCMsh2/Tgfbr2* mice presented distinct macroscopic and histological features. While *VCMsh2/Tgfbr2* mice developed mucinous adenocarcinomas similar to the CRCs during spontaneous tumor development (Figure 11*A*-I, II), *VCMsh2* mice developed mainly adenomas with a polyp-like appearance and low mucinous content (Figure 11*B*-I, II). All DSS-induced CRCs in *VCMsh2* mice showed nuclear beta-catenin accumulation (n = 5) (Figure 11*B*-III), while none of the DSS-induced *VCMsh2/Tgfbr2* CRCs showed nuclear beta-catenin (n = 5) (Figure 11*A*-III). These results demonstrate that both TGFBR2 signaling and a stable SPF environment protect from DSS-induced dMMR colorectal tumorigenesis.

TGFBR2 Loss and the Microbial Ecosystem Cause Distinct Dysbiotic Shifts During DSS-Induced CRC Development

Because the DSS-induced CRCs in *VCMsh2* and *VCMsh2/Tgfbr2* mice display distinct phenotypic and molecular characteristics, we investigated whether they were associated with specific dynamic changes in the fecal microbiota. At 8 weeks of age, before DSS treatment, β-diversity analysis revealed significant separation of *VCMsh2* and *VCMsh2/Tgfbr2* microbiota with a low dissimilarity value (Figure 12*A*, Table 18 in Figure 12). After DSS-induced CRC development, the microbiota in the 2 mouse lines separated by a considerably greater dissimilarity value (Figure 12*A*, Table 18 in Figure 12) indicating that the TGFBR2 status has a significant impact on microbiota development over time. Specifically, DSS-induced CRC tumorigenesis was associated with a significant reduction in α-diversity in *VCMsh2/Tgfbr2* mice but not in *VCMsh2* mice (Figure 12*B*). β-Diversity measured by Bray-Curtis principal components metrics revealed significant differences in the microbiota in DSS-treated *VCMsh2/Tgfbr2* mice compared with their pretreatment composition (Figure 12*C*, Table 18 in Figure 12). Although DSS also caused a significant separation of microbiota in *VCMsh2* mice, the observed dissimilarity between untreated and treated mice was much lower (Figure 12*D*, Table 18 in Figure 12).

The taxon composition in response to DSS-induced CRC within both mouse lines showed distinct genera expansion–contraction profiles (Figure 13*A* and *B*). The microbiota in DSS-treated *VCMsh2/Tgfbr2* mice with mucinous CRCs were characterized by significant increases in the proportional abundances of *Bacteroides*, *Parabacteroides*, *Akkermansia*, and *Desulfovibrio* (Figure 13*A*). In contrast, *VCMsh2* mice with nonmucinous CRCs showed pronounced abundance in *Alistipes*, *Escherichia/Shigella*, and *Turicibacter* genera but only a minimal increase in *Akkermansia* (Figure 13*B*). We also observed a reduction of distinct genera in both mouse lines: *VCMsh2/Tgfbr2* microbiota were characterized by reductions in *Lactobacillus* and *Rikenella* abundance, whereas *VCMsh2* mice mainly showed reduction in *Barnesiella* and *Enterohabdus* abundance (Figure 13*A* and *B*).

Finally, we tested how DSS treatment affected the microbiota composition specific to CRC development in the restricted SPF environment. No reduction of α-diversity in *VCMsh2/Tgfbr2-SPF* microbiota was evident (Figure 13*C*), with only a discrete but significant difference in β-diversity (Figure 13*D*). The genera significantly affected by DSS

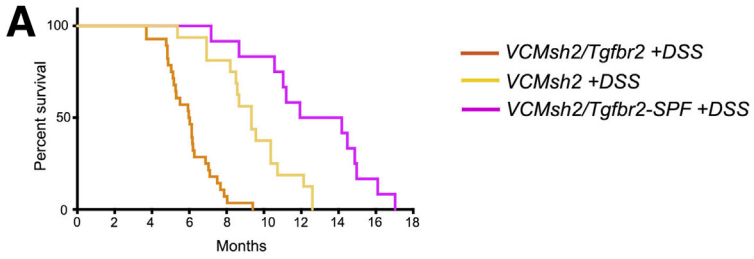

Table 16. Comparison of tumor incidence

Genotype	N	Mice with colon tumor	Mice with SI tumor	Mice with colon + SI tumor	Mice with no tumor
VCMsh2/Tgfbr2 +DSS	20	15 (75%)	0	5 (25%)	0
VCMsh2 +DSS	16	5 (31.25%)	5 (31.25%)	4 (25%)	2 (12.5%)
VCMsh2/Tgfbr2 -SPF +DSS	15	5 (33.4%)	4 (26.6%)	3 (20%)	3 (20%)

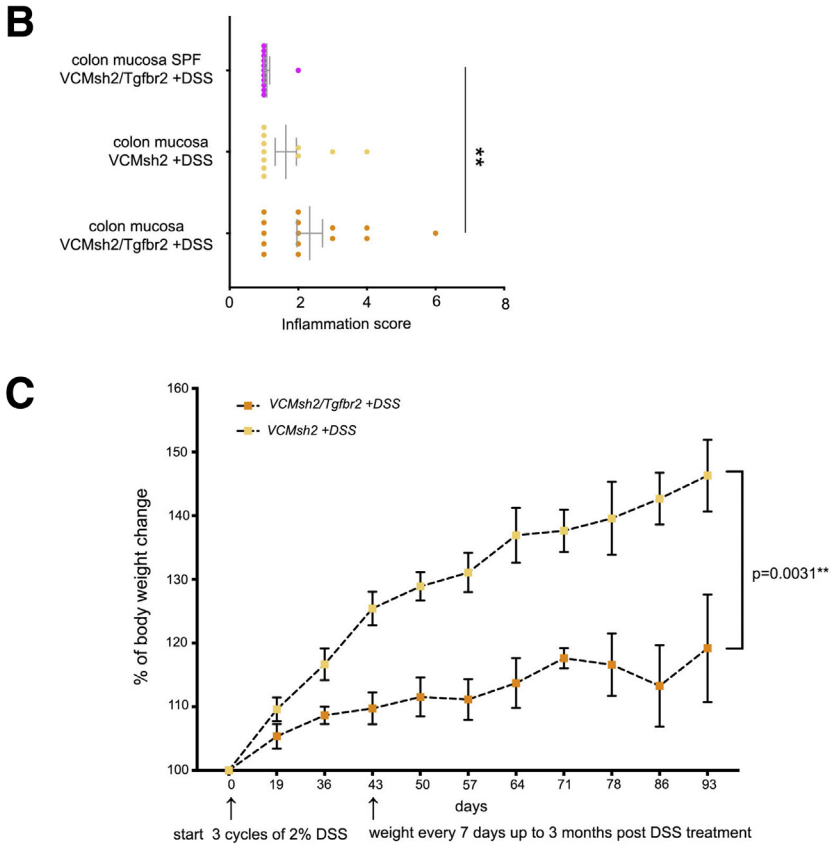

Figure 10. *Tgfbr2* status and microbiota composition modulate DSS-induced colonic inflammation and dMMR colorectal tumorigenesis. (*A*) Kaplan-Meier analysis. *VCMsh2/Tgfbr2* + DSS (n = 20) vs *VCMsh2* +DSS (n = 16), $P < .0001$; *VCMsh2/Tgfbr2* +DSS vs *VCMsh2/Tgfbr2-SPF* +DSS (n = 15), $P < .0001$. (*B*) Inflammation score. *VCMsh2/Tgfbr2* +DSS (n = 15) vs *VCMsh2/Tgfbr2-SPF* +DSS (n = 12), $^{**}P = .005$. (*C*) Long-term body weight recovery during or after DSS treatment recorded every 7 days. *VCMsh2* mice (n = 6), *VCMsh2/Tgfbr2* mice (n = 13). Weight is shown as relative to the initial body weight, $^{**}P = .007$.

treatment of *VCMsh2/Tgfbr2-SPF* mice included a significant increase in *Escherichia/Shigella* together with a significant decrease in *Mucispirillum* and *Roseburia* (Figure 13*E*). When the microbiota in DSS-treated *VCMsh2/Tgfbr2* mice was compared with that of DSS-treated *VCMsh2* or *VCMsh2/Tgfbr2-SPF* mice, an increase in *Bacteroides* and *Parabacteroides* but not in *Escherichia/Shigella* appeared to be a distinctive feature of IBD-CRC development in *VCMsh2/Tgfbr2* mice (Figure 13*F* and *G*).

Discussion

In the gastrointestinal tract, TGFB signaling plays a central role in the control of cell growth and differentiation, the maintenance of intestinal homeostasis and, importantly, can either promote or suppress inflammation and cancer formation.[8] Indeed, disruptive mutations in several TGFB signaling pathway factors are found in human CRCs and colitis-associated CRCs.[41] The aim of the current study was to determine how TGFBR2 mutations that occur at high

Table 17. Comparison of tumor incidence

Genotype	N	Number of colon tumors 12 days post DSS	N	Number of colon tumors 30 days post DSS
VCMsh2/Tgfbr2 +DSS	5	4 adenocarcinoma	5	6 adenocarcinoma
VCMsh2 +DSS	3	1 adenoma	4	0

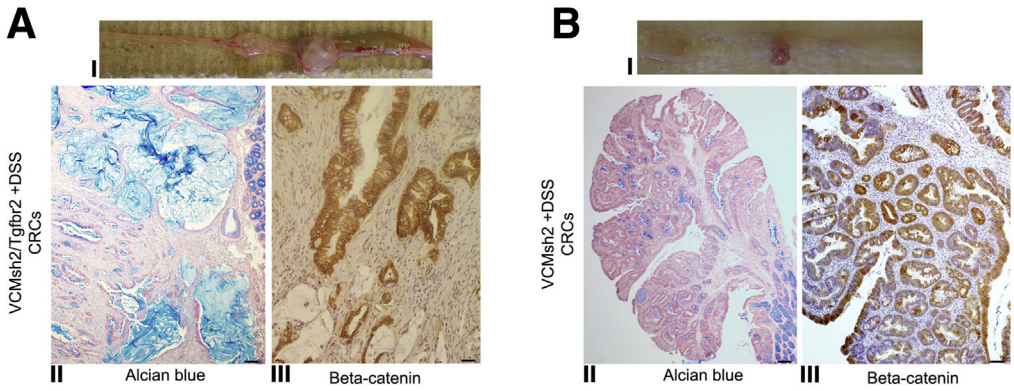

Figure 11. The effect of *Tgfbr2* loss of function in DSS-induced dMMR CRCs. (*A*) CRCs in *VCMsh2/Tgfbr2* mice treated with DSS (objectives magnification): I, macroscopic mucinous CRCs. II, Alcian blue staining showing blue mucin lakes (scale bar = 200 μm). III, Beta-catenin membrane-bound staining (scale bar = 50 μm). (*B*) CRCs in *VCMsh2* mice treated with DSS. I, CRC with a polyp-like appearance. II, Alcian blue staining showing prominent villous or tubulovillous histology and absence of mucin lakes (scale bar = 200 μm). III, Beta-catenin nuclear accumulation (scale bar = 50 μm).

frequency in MSI-CRCs affect histological and molecular features of dMMR-driven colon tumorigenesis in an animal model. The loss of TGFBR2 signaling in *VCMsh2/Tgfbr2* mice not only induced a mucinous phenotype in intestinal dMMR tumors, but also increased intestinal inflammation and the susceptibility to CRCs with histopathological features characteristic of human IBD-CRCs. The mutational spectra and gene expression profiles in *VCMsh2/Tgfbr2* CRCs indicated that the combined effects of dMMR and loss of TGFBR2 signaling led to the disruption of intestinal homeostasis during the development of IBD-CRCs. The gene expression changes in *VCMsh2/Tgfbr2* CRCs indicate that several genes and pathways could be candidates for further investigation in preclinical studies. Importantly, an SPF environment had a protective effect lowering the incidence of *VCMsh2/Tgfbr2* IBD-CRCs, suggesting that elements of the gut microbiota play a crucial role in the development of these tumors.

The microenvironment of *VCMsh2/Tgfbr2* IBD-CRCs displayed increased immune cell infiltration and proinflammatory cytokine release including IL-6, TNF-α, and IL-17A, similar to human IBD-CRCs. Inflammatory processes induce oxidative DNA damage, which in part is repaired by MMR.[20] Consistent with this, the mutational spectra in *VCMsh2/Tgfbr2* IBD-CRCs were representative of not only unrepaired replication errors but also unrepaired oxidative DNA lesions. The IBD-CRCs in *VCMsh2/Tgfbr2* mice showed no *Apc* mutations either during spontaneous or DSS-induced colorectal tumorigenesis in contrast to the DSS-induced CRCs in *VCMsh2* mice or SI tumors in both mouse lines. This is reminiscent of most IBD-CRCs in human patients that do not harbor *APC* mutations or seem to acquire them at later stages during tumor development and indicates that TGFBR2 loss at the early stages of tumorigenesis is crucial for their etiology or progression.[15,17] However, other genes with known roles in intestinal homeostasis or colorectal tumorigenesis carried mutations in *VCMsh2/Tgfbr2* CRCs. These include mutations in the PPARα/RXRα pathway, which plays a protective role against inflammation and colitis-associated colorectal tumorigenesis.[42,43] Mutations in *Ctnnd1*, *Acvr2a/1b*, and *Hnf1*α were also found, suggesting that the loss of intestinal epithelial adherens junction signaling integrity is a feature in dMMR IBD-CRCs.[26,44,45] Overall, the mutational landscape in *VCMsh2/Tgfbr2* IBD-CRCs shared significant similarities with human MSI-positive CRCs and included many genetic alterations that were reported in human IBD-CRCs or mouse models of colitis, such as mutations in *Nrlp6*, *Arid1a*, *Kmt2c*, and *Sirt1*.[37,46,47]

IPA bio-function analysis revealed several gene expression changes specific to *VCMsh2/Tgfbr2* CRCs. For example, genes involved in liver fibrosis were upregulated, suggesting a role for fibrosis in remodeling the tumor microenvironment during prolonged inflammation in *VCMsh2/Tgfbr2* IBD-CRCs.[48,49] Widespread expression of iNOS/NOS2 in *VCMsh2/Tgfbr2* IBD-CRCs (Table 11 in Figure 6, Figure 6*F*) was observed reminiscent of elevated iNOS expression in human IBD-affected intestines.[50] The IBD-CRC microenvironment also shared significant similarities with the gene expression signature of human fibroblasts exposed to TGFB1 (Figure 6*D* and *E*), which is also found in CRC patients at higher risk of relapse after therapy.[51] These results are consistent with the notion that while TGFB signaling suppresses the initiation of tumorigenesis in intestinal epithelial cells,[10] at later stages, the increased release of

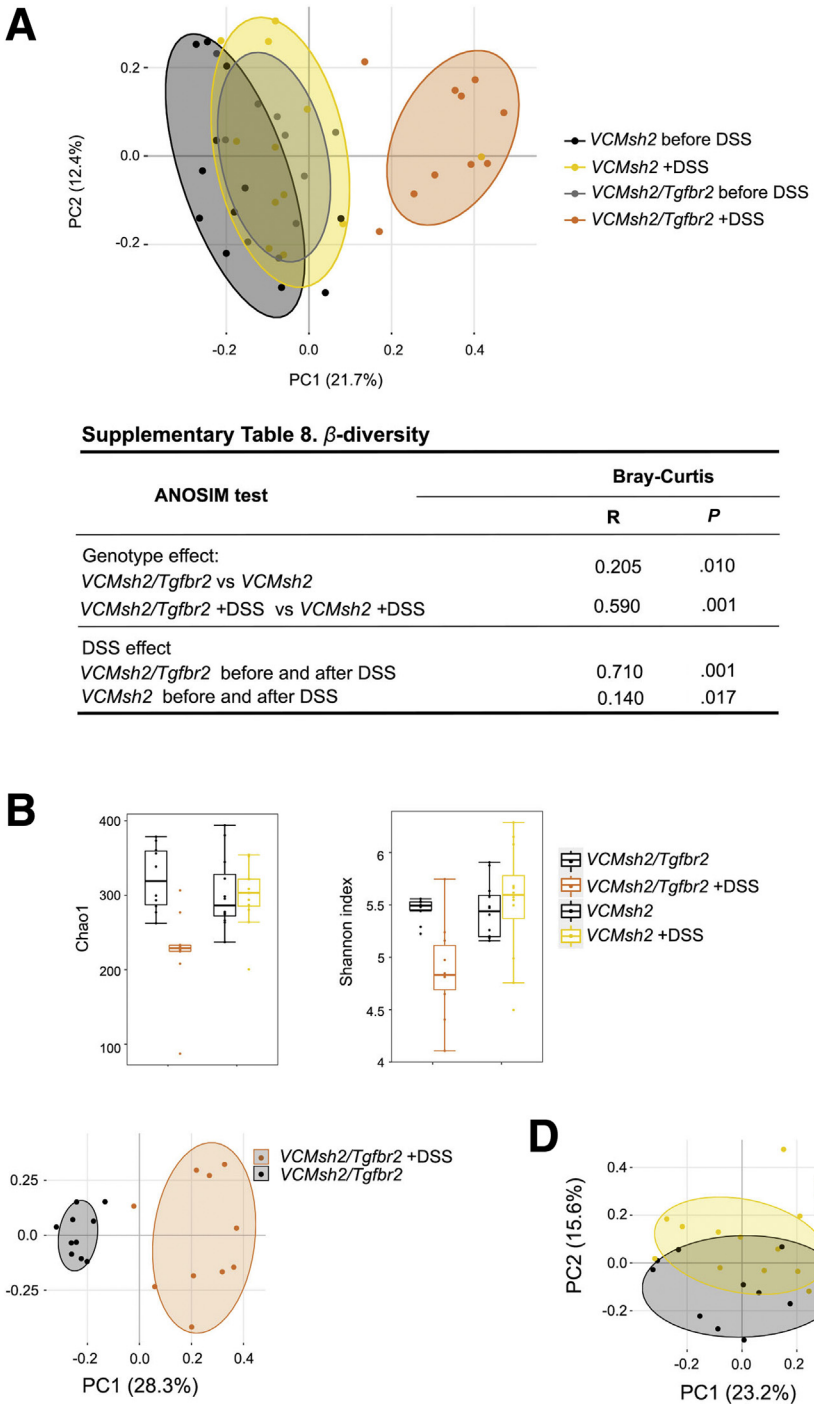

Supplementary Table 8. β-diversity

ANOSIM test	Bray-Curtis	
	R	*P*
Genotype effect:		
VCMsh2/Tgfbr2 vs *VCMsh2*	0.205	.010
VCMsh2/Tgfbr2 +DSS vs *VCMsh2* +DSS	0.590	.001
DSS effect		
VCMsh2/Tgfbr2 before and after DSS	0.710	.001
VCMsh2 before and after DSS	0.140	.017

Figure 12. *Tgfbr2* loss and the microbial ecosystem cause distinct dysbiotic shifts during DSS-induced CRC development. (*A*) Principal coordinate (PC) analysis plots of β-diversity analysis based on Bray-Curtis metrics comparing *VCMsh2/Tgfbr2* and *VCMsh2* mice before and after DSS treatment. Significances are shown in Table 18. (*B*) α-Diversity measured before and after DSS treatment: *VCMsh2/Tgfbr2* mice: Chao1 index, $P = .002$; Shannon index, $P = .014$; *VCMsh2* mice $P > .05$ (ns). (*C*, *D*) β-diversity by PC analysis of Bray-Curtis dissimilarity distances showing a significant separation before and after DSS treatment in *VCMsh2/Tgfbr2* and in *VCMsh2*. Analyses of similarities test statistics in Table 18.

TGFB by malignant and noncancer cells within the tumor microenvironment can promote cancer progression/invasion and therapeutic resistance.[52]

Several in vitro studies tested the concept of restoring TGFBR2 signaling in microsatellite unstable CRC cell lines to suppress tumorigenesis but observed different outcomes.[30,53,54] While some studies found it reduced tumorigenicity, another study observed an increase in metastatic potential. A limitation of these studies is that they were mainly performed *in vitro*, and therefore the effect of Tgfbr2 restoration in CRC cells within the native tumor microenvironment has not been tested. It is also likely that restoration of TGFBR2 signaling at late stages in tumorigenesis will have protumorigenic effects or not be able to overcome the effects of existing mutations in tumor driver genes or the impact of severe inflammation and microbial dysbiosis that are associated with MSI-high IBD-CRCs development.

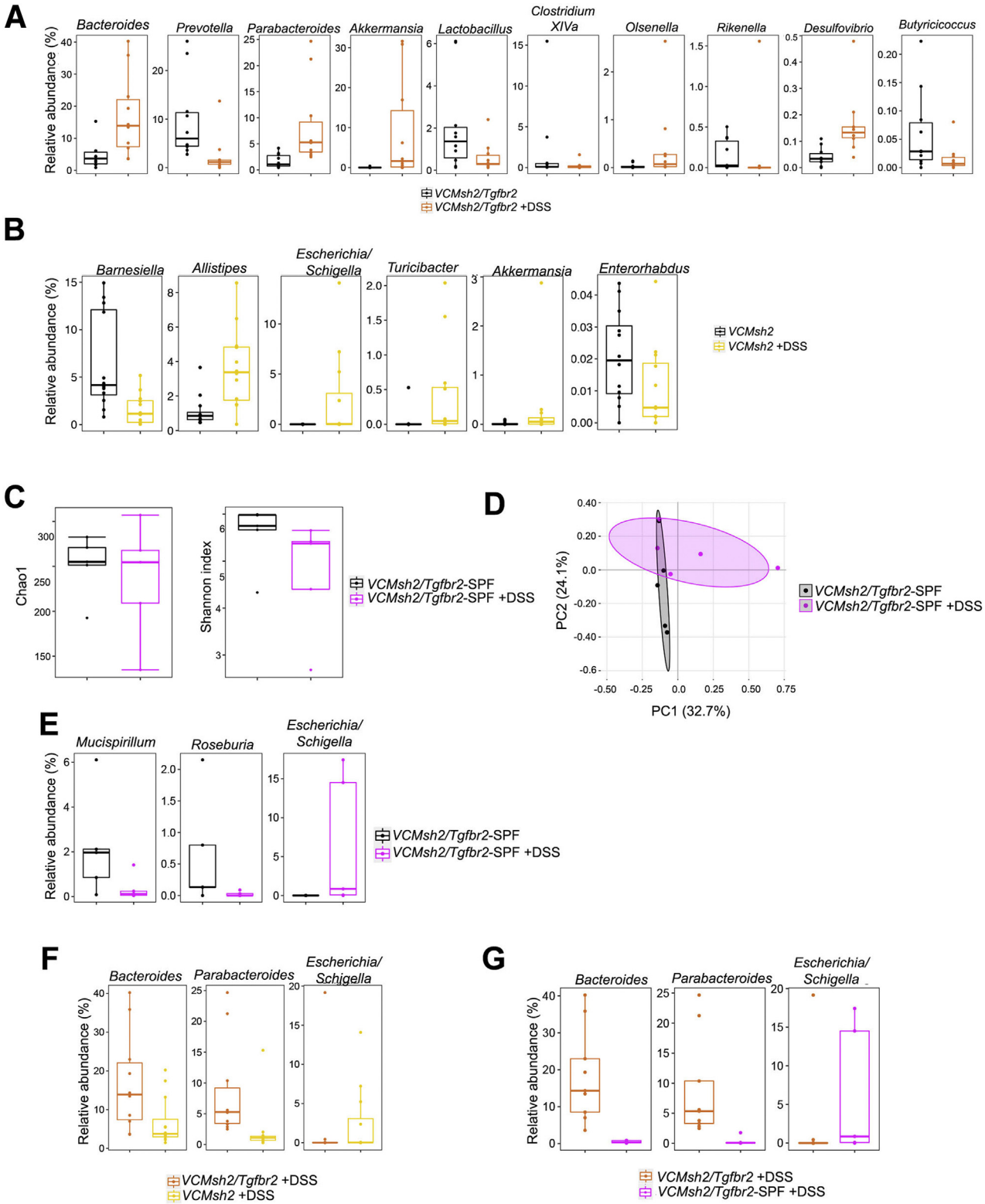

Figure 13. Dysbiotic shifts during DSS-induced *VCMsh2/Tgfbr2* tumorigenesis. (*A*, *B*) Box plots showing the relative abundance of genera significantly different after DSS treatment in *VCMsh2/Tgfbr2* mice and *VCMsh2* mice. (*C*) No significant differences in α-diversity in *VCMsh2/Tgfbr2-SPF* mice before and after DSS treatment. (*D*) Principal coordinate (PC) analysis plots of β-diversity analysis based on Bray-Curtis metrics in *VCMsh2/Tgfbr2-SPF* before and after DSS treatment, analyses of similarities R = 0.26, P = .033. (*E*) Bar plots showing the relative abundance of genera significantly different after DSS treatment in *VCMsh2/Tgfbr2-SPF* mice. (*F*, *G*) Box plots of relative abundance comparing DSS-treated *VCMsh2/Tgfbr2* mice with either DSS-treated *VCMsh2* or *VCMsh2/Tgfbr2-SPF* mice, indicating common genera shifts signature (Supplementary Excel File S12).

The transcriptional signatures also indicated that the loss of MMR and TGFBR2 signaling had a disruptive impact on the overall functionality of epithelial CRC cells. This included changes in genes regulating intestinal stem cell fate: for example, *Cdx2*, a transcriptional regulator of cell fate specification and differentiation,[55] and *Spdef*, which controls the differentiation and maturation of goblet cells.[31] Changes in the expression of genes involved in intestinal epithelium permeability (*Cftr*, *Slc4a4*, *Sult1a1*, *Aqp1*, *Cldn15*)[32–36,56] indicate damage to the epithelial barrier as seen in human IBD epithelia. *Nlrp6* was mutated or down-regulated in *VCMsh2/Tgfbr2* CRCs (Figures 4*C* and 7*B*). *Nlrp6* is of particular interest since *Nlrp6* knockout mice show increased susceptibility to chemically induced colitis and inflammation-associated intestinal tumorigenesis.[37] Interestingly, *Nlrp6* knockout mice display enrichment of *A. muciniphila*[57] similar to *VCMsh2/Tgfbr2* IBD-CRCs. *A. muciniphila* is the only known species of the *Akkermansia* genus in mice and humans with a mucin degrading activity, suggesting that this bacterium finds a favorable environment in the mucinous IBD-CRCs in *VCMsh2/Tgfbr2* mice, which supports the hypothesis that specific genetic alterations induce a unique CRC microenvironment and thus modulate microbiota composition.[4]

The colonic mucosa in *VCMsh2/Tgfbr2* mice was more inflamed compared with their SI mucosa, which could be linked to the more dense and complex microbial communities in the colonic tract and the presence of pathobiont bacteria,[4] gut species that exert pathogenic effects in particular genetic or environmental contexts. A critical role for pathogenic genera such as *Helicobacter* and *Desulfovibrio* in the development of *VCMsh2/Tgfbr2* IBD-CRCs was observed by housing mice in an SPF environment devoid of these bacterial genera, which significantly reduced CRC incidence and increased survival. A recent study analyzing the effect of nonsteroidal anti-inflammatory drugs on intestinal tumorigenesis in another *VCMsh2/Tgfbr2* mouse line did not report increased intestinal inflammation or development of IBD-CRCs.[58] While no molecular analyses of intestinal tumors or microbiota were reported, the absence of IBD-CRCs in this mouse line could be caused by differences in microbiota composition in different animal facilities. For example, different *Smad3* knockout mouse lines displayed different CRC phenotypes, which were proposed to be caused by the presence or absence of specific pathogenic microbiota members such as *H. hepaticus*.[59–61] Recent studies have suggested more complex interactions with entire communities of pathogenic bacteria being responsible for the observed CRC phenotypes.[4] Interestingly, while the inactivation of *Tgfbr2* was reported to not cause the development of CRC in other studies,[10,62] we found that a small number of *VCTgfbr2* mice that we generated during our experiments developed mucinous CRCs (Figure 1*C*-VI), further indicating the impact of pathogenic bacteria in the conventional microbiota on CRC development. However, while some *VCMsh2/Tgfβr2* mice in the conventional barrier did not develop IBD-CRCs and the IBD-CRC incidence varied over time in our experiments, *VCMsh2/Tgfβr2-SPF* mice that developed IBD-CRCs displayed higher inflammation scores compared with mice that did not develop these tumors. This suggests that besides the microbiota, other factors, such as diet or genetic background, that can affect inflammatory processes in the colon are likely also involved in IBD-CRC development.

The analysis of microbiota alterations under DSS-induced colitogenic conditions using global metrics such as α- and β-diversity, and taxonomic analyses, provided insights into how comparable levels of intestinal epithelial damage can affect microbial dysbiosis depending on the *Tgfbr2* genotype or the baseline microbial composition. Neither α-diversity nor β-diversity was greatly affected during DSS-induced colorectal carcinogenesis in TGFBR2-expressing *VCMsh2* mice or when TGFBR2-deficient *VCMsh2/Tgfbr2* mice were housed under SPF condition. This analysis also identified specific genera that characterize the microbiota signatures in the different mouse lines during CRC development: while DSS-induced CRCs in *VCMsh2/Tgfbr2* mice were associated with a marked increase in the abundance of *Akkermansia*, *Desulfovibrio*, *Bacteroides*, and *Parabacteroides*, DSS-induced CRCs in both *VCMsh2* and *VCMsh2/Tgfbr2-SPF* mice were associated with a pronounced enrichment of *Escherichia/Shigella*.[63] This suggests that the DSS-induced epithelial damage that ultimately enhances exposure to luminal microbes and induces intestinal inflammation is modulated by both the synergistic effects of *Msh2* and *Tgfbr2* inactivation and the initial microbiota composition. Similar to these findings in IBD-CRC bearing *VCMsh2/Tgfbr2* mice, both fecal and mucosal biopsies in LS patients with colorectal adenomas contained increased abundance in *Desulfovibrio*.[64] Interestingly, a role for this microbe in inducing proinflammatory responses and DNA damage has been proposed.[65] This study also found similar to *VCMsh2/Tgfbr2* mice (Figure 9*E*) an association between *MSH2* mutations and enrichment in *Coprobacillus*.

In summary, these data indicate that the loss of MMR and TGFBR2 signaling can play crucial roles in IBD-CRC and that *Tgfbr2* inactivation has a significant impact on both the histopathologic and molecular characteristics of dMMR CRCs. The loss of TGFBR2 early during dMMR IBD-CRC development appears to be crucial affecting the underlying tumorigenic pathways that do not involve canonical WNT-driven tumorigenesis, but rather involve novel mutations, many of which also occur in human IBD-CRCs. MSI-high ulcerative colitis–CRCs showed a high frequency of *TGFBR2* mutations in dysplastic lesions[15] potentially being early precancerous lesions, and therefore the early loss of TGFBR2 in the context of dMMR might be critical in their transformation into IBD-CRC. The baseline microbiota composition had a significant impact on dMMR colorectal tumorigenesis in *VCMsh2/Tgfbr2* mice, indicating that TGFBR2 inactivation in conjunction with an inflammatory or oncogenic microbiota determines the level of inflammation and IBD-CRC development, which in turn is associated with specific genera shifts. Therefore, as in *VCMsh2/Tgfbr2* mice, it is possible that the TGFBR2 status together with the mutational profile in MSI-high IBD-CRCs in human patients

will not only affect their histopathological features and the associated microbiota, but also may ultimately have important implications for diagnosis and treatment of these tumors.

Materials and Methods

Animal Models

Msh2^{loxP} mice were described previously.[66] *Villin-Cre* transgenic mice were obtained from the Jackson Laboratory (Bar Harbor, ME) (*B6:D2-Tg Villin-Cre*). *Tgfbr2*^{loxP} and *Fabp1-Cre* mice were obtained from the National Cancer Institute Frederick Mouse Repository (strain code: *01XN5; B6.129S6* and *01XD8; FVB/N*, respectively).[67,68] All mice were genotyped by PCR as previously described[66–68] and kept in conventional housing conditions under animal use protocol 00001194 approved by the Institutional Animal Care and Use Committee at the Albert Einstein College of Medicine.

To conditionally inactivate the *Msh2*^{loxP} and *Tgfbr2*^{loxP} genes in the intestinal epithelium, mice of each line were individually mated with *Villin-Cre* mice. *Villin-Cre;Msh2*$^{loxP/loxP}$ (*VCMsh2*) or *Villin-Cre;Tgfbr2*$^{loxP/loxP}$ (*VCTgfbr2*) mice were mated to create *VCMsh2*$^{loxP/loxP}$*;Tgfbr2*$^{/loxP/loxP}$ (*VCMsh2/Tgfbr2*) mice. *Fabp1-Cre;Msh2*$^{loxP/loxP}$*;Tgfbr2*$^{/loxP/loxP}$ (*FCMsh2/Tgfbr2*) mice were generated in a similar manner. *VCMsh2/Tgfbr2-SPF* mice were rederived into SPF foster mothers (Swiss Webster Restricted Flora Taconic) and aged in isolators. These SPF mice are certified free of rodent pathogens in addition to the opportunistic *Klebsiella pneumoniae*, *Staphylococcus aureus*, *Pseudomonas aeruginosa*, *beta hemolytic Streptococcus* and *Pasteurella multocida*. Animals in the conventional barrier were fed standard PicoLab Mouse Diet 20 5058 (Lab Supply, Northlake, TX) and animals in the SPF barrier were fed Laboratory Autoclavable Rodent Diet 5010 (LabDiet, St Louis, MO). For all experiments, approximately equal numbers of male and female mice were analyzed. Moribund mice were euthanized and the number and location of tumors was recorded.

Animal Experiments

For DSS treatment experiments, 8-week-old *VCMsh2/Tgfbr2* and *VCMsh2* mice were provided with drinking water containing 2% of DSS (colitis grade; MP Biomedicals, Santa Ana, CA) ad libitum for 5 days in 3 cycles alternated by 2 weeks' recovery. Mice weight was measured after each cycle or recovery cycle and every 7 days post–DSS treatment for up to 3 months.

Tissue Processing

Formalin-fixed paraffin embedded sections were prepared for hematoxylin and eosin and antibodies staining. Pathological examination conducted blindly by a board-certified veterinary pathologist to assess tumor presence and inflammation score of mucosa and submucosa.[69]

Tissue staining using anti-beta-catenin and anti-TNF-α antibodies was performed following the Vectastatin ABC Kit protocol using a pH 6 citrate buffer (Vector Laboratories, Newark, CA) for antigen retrieval. Alcian blue staining was performed using the Vector lab kit. A Zeiss Axioskop 2 equipped with an AxioCam camera and ZEN imaging software (Zeiss, Wetzlar, Germany) were used to acquire IHC and hematoxylin and eosin images.

8-oxoG IHC Staining

The analysis of 8-oxoG by IHC was conducted by standard procedures. The antigen retrieval step was substituted by a permeabilization step performed by incubating the slides for 15 minutes in 0.1% Triton X-100 (Bio-Rad, Hercules, CA) in phosphate-buffered saline. Ribonucleic acids were removed by incubation in 20 μg/mL DNase-free RNase solution (Qiagen, Hilden, Germany) at 37°C for 1 hour. Sections were then treated at room temperature for 10 minutes with 10-μg/mL Proteinase K (Promega, Madison, WI). To denature tissue DNA sections were incubated in 2N HCl at room temperature for 5 minutes, neutralized in a mixture of 2N HCl and 1M Tris (1:2.5 v/v) for 5 minutes, sections were then incubated overnight with primary anti-8-oxoG antibody.

8-oxoG ELISA

OxiSelect Oxidative DNA damage ELISA kit (Cell Biolabs, San Diego, CA) was used to detect and quantify 8-oxoG lesions in genomic DNA. The quantity of 8-oxoG in samples was determined by comparing absorbance to an 8-oxoG predetermined standard curve. Briefly, the 8-oxoG test samples or the 8-oxoG standards were first added to an 8-oxoG conjugate-coated plate. After a brief incubation, an anti-8-oxoG monoclonal antibody was added, followed by a horseradish conjugated peroxidase secondary antibody. The absorbance was measured at 450 nm using a plate reader. All steps were performed according to the manufacturer instructions. Values were normalized to adjacent tumor-free mucosa.

MSI Analysis

MSI was evaluated by standard procedures using a panel of 3 microsatellite markers previously published[70] in which each primer set contained 1 FITC-labeled primer. The amplification products were diluted 1:20 in water, and 2 μL of the diluted product was added to 7.5 μL of HiDi Formamide mixed with 0.5 μL of Genescan Liz 600 size standard (Life Technologies, Carlsbad, CA) in a 96-well PCR plate. This reaction mixture was denatured at 95°C for 3 minutes and rapidly chilled to 4°C. The plate was loaded onto a 3730 DNA Analyzer (Life Technologies, Carlsbad, CA) for separation via capillary electrophoresis and data collection. The raw data (.fsa files) were analyzed with GeneMarker Software (SoftGenetics, State College, PA). MSI was defined by comparing tumors and matched normal mucosa and scoring for differences in peaks

Statistical Analysis

Values are expressed as mean ± SEM. The 2-tailed, unpaired, nonparametric Mann-Whitney test was used to

evaluate significance between samples. Survival distributions were statistically compared by log-rank (Mantel-Cox) test.

Exome Sequencing

DNA was extracted from tumor and matched liver tissue using the DNA tissue extraction Kit (Qiagen) and evaluated for quality using the Pico green kit following the manufacturer instructions. Library preparation, exome sequencing and analysis were performed using standardized methods.

Genomic libraries from tumors and individually matched germline (liver) DNA were generated, enriched for exonic sequences using Agilent's SureSelect Mouse All Exon V1 target enrichment kit (S0276129; Agilent, Santa Clara, CA) and sequenced using Illumina NovaSeq6000 S4 (2 × 150bp; Illumina, San Diego, CA). Design files describing enriched regions were converted from mm9 to mm10 coordinates using the UCSC online tool hgLiftOver. Raw fastq files were downloaded from the Psomagen server and file integrity confirmed by md5sum value.

Flanking adapters were removed (Trim Galore, v0.3.7; https://github.com/FelixKrueger/TrimGalore) and sequence quality assessed (FastQC v0.11.4; Fastq Screen v0.4.4,and summarized with MultiQC v1.7; https://www.bioinformatics.babraham.ac.uk/projects/fastqc/, https://www.bioinformatics.babraham.ac.uk/projects/fastq_screen/).[71] Reads were aligned to the mouse mm10 genome (bwa mem v0.7.15; http://bio-bwa.sourceforge.net/bwa.shtml); initial bam files were sorted and duplicates marked (Picard modules SortSam and MarkDuplicates v2.17.1; https://broadinstitute.github.io/picard/) and then filtered to retain properly paired reads with a MAPQ value ≥10 (samtools view v1.9).[72]

Average coverage in the filtered bam files, over enriched regions described in the design file, was between 95x and 125x (GATK module DepthOfCoverage v4.1.7.0.[73] BQSR (base quality score recalibration) bam files were generated from the filtered bam files (GATK modules BaseRecalibrator and ApplyBQSR) and used as input for somatic variant calling. For each tumor–liver matched pair, somatic variants were initially identified using 3 variant callers, Mutect2 (GATK v4.1.7.0),[73] Strelka2 (v2.9.10; assisted by Manta v1.6.0),[74] and Lancet (v1.1.0).[75] For each tumor–liver pair, pass-filter somatic variants identified by at least 2 of the variant callers (determined with bcftools module isec v1.9; http://www.htslib.org/doc/bcftools.html) were retained for further analysis and annotated using SnpEff[76] and further manipulated using SnpSift (v4.3T).[77] Data visualization was done using the MAFtools package.[78] The cBioPortal platform was employed to analyze human mutation frequencies in MSI or MSS CRCs, combining all the available datasets from the bowel group.[23,79] A full list of mutations for each sample is available in Supplementary Excel File S1. A full list of selected mutations from Din et al[26] is available in Supplementary Excel File S2. IPA Bio-profile analysis list of genes previously found associated with colitis and/or IBD-CRC is shown in Supplementary Excel File S3.

BioProject accession number for exome sequencing data: PRJNA760488.

Quantitative PCR

RNA extracted from tumor and tumor-free mucosa was used to synthetize complementary DNA using the SuperScript enzyme protocol (Invitrogen, Carlsbad, CA). VeriQuest SYBR Green PCR mix (Affymetrix, Santa Clara, CA) was used. Ribosomal U6 internal control was used to normalize the relative expression of each messenger RNA. Primers were used from previously published studies or designed to span 2 adjacent exons. Each sample was measured at least twice using a ViiA7 machine (Thermo Fisher Scientific, Waltham, MA). Data are expressed as fold change relative to wild-type (Supplementary Excel File S12).

Gene Expression Analysis

RNA was isolated from tumor and adjacent tumor-free colon mucosa using the RNeasy Mini-Kit (Qiagen). RNA extraction from sorted epithelial intestinal cells was performed using the RNeasy Plus Micro Kit (Qiagen). RNA quantity was determined using a 2100 Bioanalyzer (Agilent).

Gene expression analysis of RNA isolated from bulk tissue or sorted epithelial cells was performed using the Mouse Gene ST 1.0 Array System (Affymetrix). Microarray data were preprocessed and analyzed using R-Bioconductor software (Version 3.14.1; R Foundation for Statistical Computing, Vienna, Austria). Raw data were background corrected and RMA normalized, and expression values calculated (oligo package) were followed by annotation with the pd.mogene.1.0.st.v1 package (Carvalho B (2015). Pd.mogene.1.0.st.v1: Platform Design Info for Affymetrix MoGene-1_0-st-v1. R package version 3.14.1). Hierarchical clustering was performed using heatmap.2 to examine the pairwise correlations among all datasets (Pearson's R^2). Statistical comparisons were made between the tumor and normal mucosal groups by linear modelling using the limma package in Bioconductor.[80,81] The output of this analysis was saved to a .GCT file (using exprs2gct) for further exploration. Genes evaluated as exhibiting significant differences in expression (as determined by the standard Volcano plot method) were subjected to further analysis for known and predicted regulatory relationships using IPA.[25] In addition, GSEA[82,83] was employed to investigate similarities with defined signatures from the GSEA Molecular Signatures database or from signatures that were extrapolated from previously published studies. Enrichment scores, normalized enrichment score, and *P* values were reported using GSEA analysis metrics.

A full list of genes is available in Supplementary Excel File S4 (bulk tissue) and S5 (sorted epithelial cells). A comprehensive list of growth factors and cytokines found to be changed in expression or predicted to be activated/inactivated by IPA upstream analysis is shown in Supplementary Excel File S6. A list of genes changed in expression involved in fibrosis is shown in Supplementary Excel File S6.

16S rRNA Amplicon Sequencing

Fecal DNA was extracted from mouse stool using the QIAamp DNA Stool Mini Kit (Qiagen). The 16S V3-V4 region was amplified using universal primers 341F=CCTACGGG NGGCWGCAG and 805R= GACTACHVGGGTATCTAATCC[84]; libraries were prepared using the Nextera XT index kit (Illumina). Sequencing was performed using the Illumina MiSeq platform (2 × 300 bp reads/mouse sample).

Bioinformatics and Statistical Analysis of 16S rRNA Sequencing Data

Microbiota composition analysis of 16S rRNA amplicon sequencing data was conducted following standard computational approaches, as previously described.[85] Paired-end sequencing reads (2 × 300 bp) were joined using FLASH version 1.2.8[86] and primers were removed using cutadapt v1.8.3. Cutadapt removes adapter sequences from high-throughput sequencing reads. EMBnet J 17, 10–12). Demultiplexing and quality filtering were performed using the QIIME package version 1.9.1.[87] Duplicated sequences and sequences out of a limited range of 373-473nt were discarded using the USEARCH v8.1.186.[88] After singleton removal, the remaining sequences were clustered into OTUs at a 97% identity level and chimera filtering was carried out with UCHIME[89] against the GOLD reference database. Taxonomic classification of representative out sequences was carried out using mothur v1.36.1[90] to genus level against the 16S rRNA reference of RDP trainset 16, and using SPINGO version 1.3[91] to species levels against the RDP v11.2 database. ToutOTU table was generated with USEARCH by mapping the quality-filtered sequences against the representative OTU sequenout. The OTU read counts were rarefied to the lowest read count in the dataset of 8244 reads for diversity calculations. A phylogenetic tree for UniFrac calculations was created using QIIME. α-Diversity indices (Shannon and Chao1) and β-diversity indices (Bray-Curtis, Weighted UniFrac, and Unweighted UniFrac) were generated using QIIME.

Statistical analysis and data visualization were carried out in R v4.0.4. Statistical differences for α-diversity were tested using Mann-Whitney *U* tests for 2 independent groups and Kruskal-Wallis tests for more than 2 independent groups. Principal coordinate analysis plots were created to explore β-diversity based on Bray-Curtis, Weighted UniFrac, and Unweighted UniFrac distance metrics using the ade4 package v1.7-15 with dudi.pco function. Two-dimensional principal coordinate analysis plots were created using the ggplot2 package v2.2.1. To test for statistical difference in β-diversity, analyses of similarities were carried out using the anosim function from the vegan package v2.5-6. The barplots showing different taxonomic level classification were created using the ggplot2 package. Taxa below 1% sample abundance and the unclassified taxa were grouped into the "other" category. Differentially abundance taxa were tested using DESeq2 package v1.30.1[92] *P* values from multiple pairwise comparisons were adjusted using the Benjamini-Hochberg method. Significance was assumed for adjusted *P* values $<.05$ if not stated otherwise.

BioProject accession number for 16S sequencing data: PRJNA759725. See Supplementary Excel File S7 for statistical analysis relative to Figure 9*A* and *C*–*E*. See Supplementary Excel File S8 for genus counts relative to Figure 9*C* and *D*. See Supplementary Excel File S9 for statistical analysis relative to Figure 9*F*. See Supplementary Excel File S10 for statistical analysis relative to Figure 13*A*, *B*, and *D*. See Supplementary Excel File S11 for statistical analysis relative to Figure 13*F* and *G*.

qPCR for A. muciniphilia Analysis

The abundance of *A. muciniphilia* was evaluated by real-time PCR using 16S species specific primers[93,94] and normalized to total bacteria 16S rRNA using universal EUB primers[95,96] Each sample was measured at least twice. For statistical analysis, analysis of variance was applied. Supplementary Excel File S12 lists all the primers[97,98] and antibodies used in this study.

References

1. Keum N, Giovannucci E. Global burden of colorectal cancer: emerging trends, risk factors and prevention strategies. Nat Rev Gastroenterol Hepatol 2019; 16:713–732.
2. Barrett M, Hand CK, Shanahan F, Murphy T, O'Toole PW. Mutagenesis by microbe: the role of the microbiota in shaping the cancer genome. Trends Cancer 2020;6:277–287.
3. Irrazabal T, Thakur BK, Kang M, Malaise Y, Streutker C, Wong EOY, Copeland J, Gryfe R, Guttman DS, Navarre WW, Martin A. Limiting oxidative DNA damage reduces microbe-induced colitis-associated colorectal cancer. Nat Commun 2020;11:1802.
4. Janney A, Powrie F, Mann EH. Host-microbiota maladaptation in colorectal cancer. Nature 2020;585:509–517.
5. Gupta D, Heinen CD. The mismatch repair-dependent DNA damage response: Mechanisms and implications. DNA Repair (Amst) 2019;78:60–69.
6. Rustgi AK. The genetics of hereditary colon cancer. Genes Dev 2007;21:2525–2538.
7. Boland CR, Goel A. Microsatellite instability in colorectal cancer. Gastroenterology 2010;138:2073–2087.e3.
8. Jung B, Staudacher JJ, Beauchamp D. Transforming growth factor beta superfamily signaling in development of colorectal cancer. Gastroenterology 2017; 152:36–52.
9. Neuzillet C, de Gramont A, Tijeras-Raballand A, de Mestier L, Cros J, Faivre S, Raymond E. Perspectives of TGF-beta inhibition in pancreatic and hepatocellular carcinomas. Oncotarget 2014;5:78–94.
10. Munoz NM, Upton M, Rojas A, Washington MK, Lin L, Chytil A, Sozmen EG, Madison BB, Pozzi A, Moon RT, Moses HL, Grady WM. Transforming growth factor beta receptor type II inactivation induces the malignant

transformation of intestinal neoplasms initiated by Apc mutation. Cancer Res 2006;66:9837–9844.
11. Trobridge P, Knoblaugh S, Washington MK, Munoz NM, Tsuchiya KD, Rojas A, Song X, Ulrich CM, Sasazuki T, Shirasawa S, Grady WM. TGF-beta receptor inactivation and mutant Kras induce intestinal neoplasms in mice via a beta-catenin-independent pathway. Gastroenterology 2009;136:1680–1688.e7.
12. Yu M, Trobridge P, Wang Y, Kanngurn S, Morris SM, Knoblaugh S, Grady WM. Inactivation of TGF-beta signaling and loss of PTEN cooperate to induce colon cancer in vivo. Oncogene 2014;33:1538–1547.
13. Oshima H, Nakayama M, Han TS, Naoi K, Ju X, Maeda Y, Robine S, Tsuchiya K, Sato T, Sato H, Taketo MM, Oshima M. Suppressing TGFbeta signaling in regenerating epithelia in an inflammatory microenvironment is sufficient to cause invasive intestinal cancer. Cancer Res 2015;75:766–776.
14. Guerrerio AL, Frischmeyer-Guerrerio PA, Huang C, Wu Y, Haritunians T, McGovern DPB, MacCarrick GL, Brant SR, Dietz HC. Increased prevalence of inflammatory bowel disease in patients with mutations in genes encoding the receptor subunits for TGFbeta. Inflamm Bowel Dis 2016;22:2058–2062.
15. Fujiwara I, Yashiro M, Kubo N, Maeda K, Hirakawa K. Ulcerative colitis-associated colorectal cancer is frequently associated with the microsatellite instability pathway. Dis Colon Rectum 2008;51:1387–1394.
16. Ihara S, Hirata Y, Koike K. TGF-beta in inflammatory bowel disease: a key regulator of immune cells, epithelium, and the intestinal microbiota. J Gastroenterol 2017; 52:777–787.
17. Souza RF, Lei J, Yin J, Appel R, Zou TT, Zhou X, Wang S, Rhyu MG, Cymes K, Chan O, Park WS, Krasna MJ, Greenwald BD, Cottrell J, Abraham JM, Simms L, Leggett B, Young J, Harpaz N, Meltzer SJ. A transforming growth factor beta 1 receptor type II mutation in ulcerative colitis-associated neoplasms. Gastroenterology 1997;112:40–45.
18. Gu S, Zaidi S, Hassan MI, Mohammad T, Malta TM, Noushmehr H, Nguyen B, Crandall KA, Srivastav J, Obias V, Lin P, Nguyen BN, Yao M, Yao R, King CH, Mazumder R, Mishra B, Rao S, Mishra L. Mutated CEACAMs disrupt transforming growth factor beta signaling and alter the intestinal microbiome to promote colorectal carcinogenesis. Gastroenterology 2020; 158:238–252.
19. Muller M, Hansmannel F, Arnone D, Choukour M, Ndiaye NC, Kokten T, Houlgatte R, Peyrin-Biroulet L. Genomic and molecular alterations in human inflammatory bowel disease-associated colorectal cancer. United European Gastroenterol J 2020;8:675–684.
20. Bridge G, Rashid S, Martin SA. DNA mismatch repair and oxidative DNA damage: implications for cancer biology and treatment. Cancers (Basel) 2014;6:1597–1614.
21. Terzic J, Grivennikov S, Karin E, Karin M. Inflammation and colon cancer. Gastroenterology 2010; 138:2101–2114.e5.
22. Alexandrov LB, Nik-Zainal S, Wedge DC, Aparicio SA, Behjati S, Biankin AV, Bignell GR, Bolli N, Borg A, Borresen-Dale AL, Boyault S, Burkhardt B, Butler AP, Caldas C, Davies HR, Desmedt C, Eils R, Eyfjord JE, Foekens JA, Greaves M, Hosoda F, Hutter B, Ilicic T, Imbeaud S, Imielinski M, Jager N, Jones DT, Jones D, Knappskog S, Kool M, Lakhani SR, Lopez-Otin C, Martin S, Munshi NC, Nakamura H, Northcott PA, Pajic M, Papaemmanuil E, Paradiso A, Pearson JV, Puente XS, Raine K, Ramakrishna M, Richardson AL, Richter J, Rosenstiel P, Schlesner M, Schumacher TN, Span PN, Teague JW, Totoki Y, Tutt AN, Valdes-Mas R, van Buuren MM, van 't Veer L, Vincent-Salomon A, Waddell N, Yates LR, Australian Pancreatic Cancer Genome Initiative, ICGC Breast Cancer Consortium, ICGC MMML-Seq Consortium, ICGC PedBrain, Zucman-Rossi J, Futreal PA, McDermott U, Lichter P, Meyerson M, Grimmond SM, Siebert R, Campo E, Shibata T, Pfister SM. Campbell PJ, Stratton MR. Signatures of mutational processes in human cancer. Nature 2013;500:415–421.
23. Cerami E, Gao J, Dogrusoz U, Gross BE, Sumer SO, Aksoy BA, Jacobsen A, Byrne CJ, Heuer ML, Larsson E, Antipin Y, Reva B, Goldberg AP, Sander C, Schultz N. The cBio cancer genomics portal: an open platform for exploring multidimensional cancer genomics data. Cancer Discov 2012;2:401–404.
24. Gao J, Aksoy BA, Dogrusoz U, Dresdner G, Gross B, Sumer SO, Sun Y, Jacobsen A, Sinha R, Larsson E, Cerami E, Sander C, Schultz N. Integrative analysis of complex cancer genomics and clinical profiles using the cBioPortal. Sci Signal 2013;6(269):pl1.
25. Kramer A, Green J, Pollard J Jr, Tugendreich S. Causal analysis approaches in Ingenuity Pathway Analysis. Bioinformatics 2014;30:523–530.
26. Din S, Wong K, Mueller MF, Oniscu A, Hewinson J, Black CJ, Miller ML, Jimenez-Sanchez A, Rabbie R, Rashid M, Satsangi J, Adams DJ, Arends MJ. Mutational analysis identifies therapeutic biomarkers in inflammatory bowel disease-associated colorectal cancers. Clin Cancer Res 2018;24:5133–5142.
27. Granlund A, Flatberg A, Ostvik AE, Drozdov I, Gustafsson BI, Kidd M, Beisvag V, Torp SH, Waldum HL, Martinsen TC, Damas JK, Espevik T, Sandvik AK. Whole genome gene expression meta-analysis of inflammatory bowel disease colon mucosa demonstrates lack of major differences between Crohn's disease and ulcerative colitis. PLoS One 2013;8:e56818.
28. Sadanandam A, Lyssiotis CA, Homicsko K, Collisson EA, Gibb WJ, Wullschleger S, Ostos LC, Lannon WA, Grotzinger C, Del Rio M, Lhermitte B, Olshen AB, Wiedenmann B, Cantley LC, Gray JW, Hanahan D. A colorectal cancer classification system that associates cellular phenotype and responses to therapy. Nat Med 2013;19:619–625.
29. Inoue S, Tsunoda T, Riku M, Ito H, Inoko A, Murakami H, Ebi M, Ogasawara N, Pastan I, Kasugai K, Kasai K, Ikeda H, Inaguma S. Diffuse mesothelin expression leads to worse prognosis through enhanced cellular proliferation in colorectal cancer. Oncol Lett 2020;19:1741–1750.
30. Wang J, Sun L, Myeroff L, Wang X, Gentry LE, Yang J, Liang J, Zborowska E, Markowitz S, Willson JKV,

Brattain MG. Demonstration that mutation of the type II transforming growth factor β receptor inactivates its tumor suppressor activity in replication error-positive colon carcinoma cells. J Biol Chem 1995;270:22044–22049.
31. Gregorieff A, Stange DE, Kujala P, Begthel H, van den Born M, Korving J, Peters PJ, Clevers H. The ets-domain transcription factor Spdef promotes maturation of goblet and paneth cells in the intestinal epithelium. Gastroenterology 2009;137:1333–1345.e1–3.
32. Wu F, Chakravarti S. Differential expression of inflammatory and fibrogenic genes and their regulation by NF-kappaB inhibition in a mouse model of chronic colitis. J Immunol 2007;179:6988–7000.
33. Moon C, Soria JC, Jang SJ, Lee J, Obaidul Hoque M, Sibony M, Trink B, Chang YS, Sidransky D, Mao L. Involvement of aquaporins in colorectal carcinogenesis. Oncogene 2003;22:6699–6703.
34. Ricanek P, Lunde LK, Frye SA, Stoen M, Nygard S, Morth JP, Rydning A, Vatn MH, Amiry-Moghaddam M, Tonjum T. Reduced expression of aquaporins in human intestinal mucosa in early stage inflammatory bowel disease. Clin Exp Gastroenterol 2015;8:49–67.
35. Mazzarelli P, Pucci S, Spagnoli LG. CLU and colon cancer. The dual face of CLU: from normal to malignant phenotype. Adv Cancer Res 2009;105:45–61.
36. Than BL, Linnekamp JF, Starr TK, Largaespada DA, Rod A, Zhang Y, Bruner V, Abrahante J, Schumann A, Luczak T, Walter J, Niemczyk A, O'Sullivan MG, Medema JP, Fijneman RJ, Meijer GA, Van den Broek E, Hodges CA, Scott PM, Vermeulen L, Cormier RT. CFTR is a tumor suppressor gene in murine and human intestinal cancer. Oncogene 2016;35(32):4179–4187.
37. Elinav E, Strowig T, Kau AL, Henao-Mejia J, Thaiss CA, Booth CJ, Peaper DR, Bertin J, Eisenbarth SC, Gordon JI, Flavell RA. NLRP6 inflammasome regulates colonic microbial ecology and risk for colitis. Cell 2011;145:745–757.
38. Dingemanse C, Belzer C, van Hijum SA, Gunthel M, Salvatori D, den Dunnen JT, Kuijper EJ, Devilee P, de Vos WM, van Ommen GB, Robanus-Maandag EC. Akkermansia muciniphila and Helicobacter typhlonius modulate intestinal tumor development in mice. Carcinogenesis 2015;36:1388–1396.
39. Lee C, Hong SN, Paik NY, Kim TJ, Kim ER, Chang DK, Kim YH. CD1d modulates colonic inflammation in NOD2-/- mice by altering the intestinal microbial composition comprising Acetatifactor muris. J Crohns Colitis 2019;13:1081–1091.
40. Candela M, Turroni S, Biagi E, Carbonero F, Rampelli S, Fiorentini C, Brigidi P. Inflammation and colorectal cancer, when microbiota-host mutualism breaks. World J Gastroenterol 2014;20:908–922.
41. Feagins LA. Role of transforming growth factor-beta in inflammatory bowel disease and colitis-associated colon cancer. Inflamm Bowel Dis 2010;16:1963–1968.
42. Ye X, Wu H, Sheng L, Liu YX, Ye F, Wang M, Zhou H, Su Y, Zhang XK. Oncogenic potential of truncated RXRalpha during colitis-associated colorectal tumorigenesis by promoting IL-6-STAT3 signaling. Nat Commun 2019;10:1463.
43. Desreumaux P, Dubuquoy L, Nutten S, Peuchmaur M, Englaro W, Schoonjans K, Derijard B, Desvergne B, Wahli W, Chambon P, Leibowitz MD, Colombel JF, Auwerx J. Attenuation of colon inflammation through activators of the retinoid X receptor (RXR)/peroxisome proliferator-activated receptor gamma (PPARgamma) heterodimer. A basis for new therapeutic strategies. J Exp Med 2001;193:827–838.
44. Colliver DW, Crawford NP, Eichenberger MR, Zacharius W, Petras RE, Stromberg AJ, Galandiuk S. Molecular profiling of ulcerative colitis-associated neoplastic progression. Exp Mol Pathol 2006;80:1–10.
45. Babeu JP, Boudreau F. Hepatocyte nuclear factor 4-alpha involvement in liver and intestinal inflammatory networks. World J Gastroenterol 2014;20:22–30.
46. Chakrabarty S, Varghese VK, Sahu P, Jayaram P, Shivakumar BM, Pai CG, Satyamoorthy K. Targeted sequencing-based analyses of candidate gene variants in ulcerative colitis-associated colorectal neoplasia. Br J Cancer 2017;117:136–143.
47. Wellman AS, Metukuri MR, Kazgan N, Xu X, Xu Q, Ren NSX, Czopik A, Shanahan MT, Kang A, Chen W, Azcarate-Peril MA, Gulati AS, Fargo DC, Guarente L, Li X. Intestinal epithelial sirtuin 1 regulates intestinal inflammation during aging in mice by altering the intestinal microbiota. Gastroenterology 2017;153:772–786.
48. Liu RM, Desai LP. Reciprocal regulation of TGF-beta and reactive oxygen species: A perverse cycle for fibrosis. Redox Biol 2015;6:565–577.
49. Chandler C, Liu T, Buckanovich R, Coffman LG. The double edge sword of fibrosis in cancer. Transl Res 2019;209:55–67.
50. Cross RK, Wilson KT. Nitric oxide in inflammatory bowel disease. Inflamm Bowel Dis 2003;9:179–189.
51. Calon A, Espinet E, Palomo-Ponce S, Tauriello DV, Iglesias M, Cespedes MV, Sevillano M, Nadal C, Jung P, Zhang XH, Byrom D, Riera A, Rossell D, Mangues R, Massague J, Sancho E, Batlle E. Dependency of colorectal cancer on a TGF-beta-driven program in stromal cells for metastasis initiation. Cancer Cell 2012;22:571–584.
52. Derynck R, Turley SJ, Akhurst RJ. TGFbeta biology in cancer progression and immunotherapy. Nat Rev Clin Oncol 2021;18:9–34.
53. MacKay SL, Auffenberg T, Tannahill CL, Ksontini R, Josephs MD, Nowak M, Moldawer LL, Copeland EM 3rd. Transfection of the type II TGF-beta receptor into colon cancer cells increases receptor expression, inhibits cell growth, and reduces the malignant phenotype. Ann Surg 1998;227:781–789.
54. Warusavitarne J, McDougall F, de Silva K, Barnetson R, Messina M, Robinson BG, Schnitzler M. Restoring TGFbeta function in microsatellite unstable (MSI-H) colorectal cancer reduces tumourigenicity but increases metastasis formation. Int J Colorectal Dis 2009;24:139–144.

55. Gao N, White P, Kaestner KH. Establishment of intestinal identity and epithelial-mesenchymal signaling by Cdx2. Dev Cell 2009;16:588–599.
56. Bujko M, Kober P, Mikula M, Ligaj M, Ostrowski J, Siedlecki JA. Expression changes of cell-cell adhesion-related genes in colorectal tumors. Oncol Lett 2015; 9:2463–2470.
57. Seregin SS, Golovchenko N, Schaf B, Chen J, Pudlo NA, Mitchell J, Baxter NT, Zhao L, Schloss PD, Martens EC, Eaton KA, Chen GY. NLRP6 protects Il10(-/-) mice from colitis by limiting colonization of Akkermansia muciniphila. Cell Rep 2017;19:2174.
58. Martin-Lopez J, Gasparini P, Coombes K, Croce CM, Boivin GP, Fishel R. Mutation of TGFbeta-RII eliminates NSAID cancer chemoprevention. Oncotarget 2018; 9:12554–12561.
59. Zhu Y, Richardson JA, Parada LF, Graff JM. Smad3 mutant mice develop metastatic colorectal cancer. Cell 1998;94:703–714.
60. Datto MB, Frederick JP, Pan L, Borton AJ, Zhuang Y, Wang XF. Targeted disruption of Smad3 reveals an essential role in transforming growth factor beta-mediated signal transduction. Mol Cell Biol 1999; 19:2495–2504.
61. Maggio-Price L, Treuting P, Zeng W, Tsang M, Bielefeldt-Ohmann H, Iritani BM. Helicobacter infection is required for inflammation and colon cancer in SMAD3-deficient mice. Cancer Res 2006;66:828–838.
62. Biswas S, Trobridge P, Romero-Gallo J, Billheimer D, Myeroff LL, Willson JK, Markowitz SD, Grady WM. Mutational inactivation of TGFBR2 in microsatellite unstable colon cancer arises from the cooperation of genomic instability and the clonal outgrowth of transforming growth factor beta resistant cells. Genes Chromosomes Cancer 2008;47:95–106.
63. Pleguezuelos-Manzano C, Puschhof J, Rosendahl Huber A, van Hoeck A, Wood HM, Nomburg J, Gurjao C, Manders F, Dalmasso G, Stege PB, Paganelli FL, Geurts MH, Beumer J, Mizutani T, Miao Y, van der Linden R, van der Elst S, Genomics England Research C, Garcia KC, Top J, Willems RJL, Giannakis M, Bonnet R, Quirke P, Meyerson M, Cuppen E, van Boxtel R, Clevers H. Mutational signature in colorectal cancer caused by genotoxic pks(+) E. coli. Nature 2020; 580:269–273.
64. Yan Y, Drew DA, Markowitz A, Lloyd-Price J, Abu-Ali G, Nguyen LH, Tran C, Chung DC, Gilpin KK, Meixell D, Parziale M, Schuck M, Patel Z, Richter JM, Kelsey PB, Garrett WS, Chan AT, Stadler ZK, Huttenhower C. Structure of the mucosal and stool microbiome in Lynch syndrome. Cell Host Microbe 2020;27:585–600.e4.
65. Hale VL, Chen J, Johnson S, Harrington SC, Yab TC, Smyrk TC, Nelson H, Boardman LA, Druliner BR, Levin TR, Rex DK, Ahnen DJ, Lance P, Ahlquist DA, Chia N. Shifts in the fecal microbiota associated with adenomatous polyps. Cancer Epidemiol Biomarkers Prev 2017;26:85–94.
66. Kucherlapati MH, Lee K, Nguyen AA, Clark AB, Hou H Jr, Rosulek A, Li H, Yang K, Fan K, Lipkin M, Bronson RT, Jelicks L, Kunkel TA, Kucherlapati R, Edelmann W. An Msh2 conditional knockout mouse for studying intestinal cancer and testing anticancer agents. Gastroenterology 2010;138:993–1002.e1.
67. Wong MH, Saam JR, Stappenbeck TS, Rexer CH, Gordon JI. Genetic mosaic analysis based on Cre recombinase and navigated laser capture microdissection. Proc Natl Acad Sci U S A 2000;97:12601–12606.
68. Chytil A, Magnuson MA, Wright CV, Moses HL. Conditional inactivation of the TGF-beta type II receptor using Cre:Lox. Genesis 2002;32:73–75.
69. Fung KY, Putoczki T. In vivo models of inflammatory bowel disease and colitis-associated cancer. In: Jenkins BJ, ed. Inflammation and Cancer: Methods and Protocols. New York, NY: Springer, 2018:3–13.
70. Woerner SM, Tosti E, Yuan YP, Kloor M, Bork P, Edelmann W, Gebert J. Detection of coding microsatellite frameshift mutations in DNA mismatch repair-deficient mouse intestinal tumors. Mol Carcinog 2015; 54:1376–1386.
71. Ewels P, Magnusson M, Lundin S, Kaller M. MultiQC: summarize analysis results for multiple tools and samples in a single report. Bioinformatics 2016; 32:3047–3048.
72. Li H, Handsaker B, Wysoker A, Fennell T, Ruan J, Homer N, Marth G, Abecasis G, Durbin R. 1000 Genome Project Data Processing Subgroup. The Sequence Alignment/Map format and SAMtools. Bioinformatics 2009;25:2078–2079.
73. McKenna A, Hanna M, Banks E, Sivachenko A, Cibulskis K, Kernytsky A, Garimella K, Altshuler D, Gabriel S, Daly M, DePristo MA. The Genome Analysis Toolkit: a MapReduce framework for analyzing next-generation DNA sequencing data. Genome Res 2010; 20:1297–1303.
74. Kim S, Scheffler K, Halpern AL, Bekritsky MA, Noh E, Kallberg M, Chen X, Kim Y, Beyter D, Krusche P, Saunders CT. Strelka2: fast and accurate calling of germline and somatic variants. Nat Methods 2018; 15:591–594.
75. Narzisi G, Corvelo A, Arora K, Bergmann EA, Shah M, Musunuri R, Emde AK, Robine N, Vacic V, Zody MC. Genome-wide somatic variant calling using localized colored de Bruijn graphs. Commun Biol 2018;1:20.
76. Cingolani P, Platts A, Wang le L, Coon M, Nguyen T, Wang L, Land SJ, Lu X, Ruden DM. A program for annotating and predicting the effects of single nucleotide polymorphisms, SnpEff: SNPs in the genome of Drosophila melanogaster strain w1118; iso-2; iso–3. Fly (Austin) 2012;6:80–92.
77. Cingolani P, Patel VM, Coon M, Nguyen T, Land SJ, Ruden DM, Lu X. Using Drosophila melanogaster as a model for genotoxic chemical mutational studies with a new program. SnpSift. Front Genet 2012;3:35.
78. Mayakonda A, Lin DC, Assenov Y, Plass C, Koeffler HP. Maftools: efficient and comprehensive analysis of somatic variants in cancer. Genome Res 2018; 28:1747–1756.
79. Dalgic A, Kandogan T, Koc M, Kulan CA, Yagci A, Engin O, Aksoy G, Ozuer MZ. Short-term laryngeal electromyography and histopathological findings after primary

reconstruction of the inferior laryngeal nerve in rabbits: prospective study. J Laryngol Otol 2013;127:48–53.
80. Gentleman RC, Carey VJ, Bates DM, Bolstad B, Dettling M, Dudoit S, Ellis B, Gautier L, Ge Y, Gentry J, Hornik K, Hothorn T, Huber W, Iacus S, Irizarry R, Leisch F, Li C, Maechler M, Rossini AJ, Sawitzki G, Smith C, Smyth G, Tierney L, Yang JY, Zhang J. Bioconductor: open software development for computational biology and bioinformatics. Genome Biol 2004;5:R80.
81. Ritchie ME, Phipson B, Wu D, Hu Y, Law CW, Shi W, Smyth GK. limma powers differential expression analyses for RNA-sequencing and microarray studies. Nucleic Acids Res 2015;43:e47.
82. Subramanian A, Tamayo P, Mootha VK, Mukherjee S, Ebert BL, Gillette MA, Paulovich A, Pomeroy SL, Golub TR, Lander ES, Mesirov JP. Gene set enrichment analysis: a knowledge-based approach for interpreting genome-wide expression profiles. Proc Natl Acad Sci U S A 2005;102:15545–15550.
83. Mootha VK, Lindgren CM, Eriksson KF, Subramanian A, Sihag S, Lehar J, Puigserver P, Carlsson E, Ridderstrale M, Laurila E, Houstis N, Daly MJ, Patterson N, Mesirov JP, Golub TR, Tamayo P, Spiegelman B, Lander ES, Hirschhorn JN, Altshuler D, Groop LC. PGC-1alpha-responsive genes involved in oxidative phosphorylation are coordinately downregulated in human diabetes. Nat Genet 2003;34:267–273.
84. Herlemann DP, Labrenz M, Jurgens K, Bertilsson S, Waniek JJ, Andersson AF. Transitions in bacterial communities along the 2000 km salinity gradient of the Baltic Sea. ISME J 2011;5:1571–1579.
85. Tran TTT, Cousin FJ, Lynch DB, Menon R, Brulc J, Brown JR, O'Herlihy E, Butto LF, Power K, Jeffery IB, O'Connor EM, O'Toole PW. Prebiotic supplementation in frail older people affects specific gut microbiota taxa but not global diversity. Microbiome 2019;7:39.
86. Magoc T, Salzberg SL. FLASH: fast length adjustment of short reads to improve genome assemblies. Bioinformatics 2011;27:2957–2963.
87. Caporaso JG, Kuczynski J, Stombaugh J, Bittinger K, Bushman FD, Costello EK, Fierer N, Pena AG, Goodrich JK, Gordon JI, Huttley GA, Kelley ST, Knights D, Koenig JE, Ley RE, Lozupone CA, McDonald D, Muegge BD, Pirrung M, Reeder J, Sevinsky JR, Turnbaugh PJ, Walters WA, Widmann J, Yatsunenko T, Zaneveld J, Knight R. QIIME allows analysis of high-throughput community sequencing data. Nat Methods 2010;7:335–336.
88. Edgar RC. Search and clustering orders of magnitude faster than BLAST. Bioinformatics 2010;26:2460–2461.
89. Edgar RC, Haas BJ, Clemente JC, Quince C, Knight R. UCHIME improves sensitivity and speed of chimera detection. Bioinformatics 2011;27:2194–2200.
90. Schloss PD, Westcott SL, Ryabin T, Hall JR, Hartmann M, Hollister EB, Lesniewski RA, Oakley BB, Parks DH, Robinson CJ, Sahl JW, Stres B, Thallinger GG, Van Horn DJ, Weber CF. Introducing mothur: open-source, platform-independent, community-supported software for describing and comparing microbial communities. Appl Environ Microbiol 2009;75:7537–7541.
91. Allard G, Ryan FJ, Jeffery IB, Claesson MJ. SPINGO: a rapid species-classifier for microbial amplicon sequences. BMC Bioinformatics 2015;16:324.
92. Love MI, Huber W, Anders S. Moderated estimation of fold change and dispersion for RNA-seq data with DESeq2. Genome Biol 2014;15:550.
93. Png CW, Linden SK, Gilshenan KS, Zoetendal EG, McSweeney CS, Sly LI, McGuckin MA, Florin TH. Mucolytic bacteria with increased prevalence in IBD mucosa augment in vitro utilization of mucin by other bacteria. Am J Gastroenterol 2010;105:2420–2428.
94. Edwards KC, Naz T, Stanton CA, Goniewicz ML, Hatsukami DK, Smith DM, Wang L, Villanti A, Pearson J, Blount BC, Bansal-Travers M, Feng J, Niaura R, Manderski MTB, Sosnoff CS, Delnevo CD, Duffy K, Del Valle-Pinero AY, Rostron BL, Everard C, Kimmel HL, van Bemmel DM, Hyland A. Urinary cotinine and cotinine + trans-3'-hydroxycotinine (TNE-2) cut-points for distinguishing tobacco use from nonuse in the United States: PATH Study (2013-2014). Cancer Epidemiol Biomarkers Prev 2021;30:1175–1184.
95. Amann RI, Binder BJ, Olson RJ, Chisholm SW, Devereux R, Stahl DA. Combination of 16S rRNA-targeted oligonucleotide probes with flow cytometry for analyzing mixed microbial populations. Appl Environ Microbiol 1990;56:1919–1925.
96. Wlodarska M, Willing B, Keeney KM, Menendez A, Bergstrom KS, Gill N, Russell SL, Vallance BA, Finlay BB. Antibiotic treatment alters the colonic mucus layer and predisposes the host to exacerbated Citrobacter rodentium-induced colitis. Infect Immun 2011;79:1536–1545.
97. Cooks T, Pateras IS, Tarcic O, Solomon H, Schetter AJ, Wilder S, Lozano G, Pikarsky E, Forshew T, Rosenfeld N, Harpaz N, Itzkowitz S, Harris CC, Rotter V, Gorgoulis VG, Oren M. Mutant p53 prolongs NF-kappaB activation and promotes chronic inflammation and inflammation-associated colorectal cancer. Cancer Cell 2013;23:634–646.
98. Katakowski JA, Mukherjee G, Wilner SE, Maier KE, Harrison MT, DiLorenzo TP, Levy M, Palliser D. Delivery of siRNAs to dendritic cells using DEC205-targeted lipid nanoparticles to inhibit immune responses. Mol Ther 2016;24:146–155.

Received October 5, 2021. Accepted May 18, 2022.

Correspondence
Address correspondence to: Elena Tosti, PhD, Department of Cell Biology, Albert Einstein College of Medicine, 1301 Morris Park Avenue, Bronx, NY 10461. e-mail: elena.tosti@einsteinmed.edu; fax: 718-430-8574; or Winfried Edelmann, PhD, Department of Cell Biology, Albert Einstein College of Medicine, 1301 Morris Park Avenue, Bronx, NY 10461. e-mail: winfried.edelmann@einsteinmed.edu; fax: 718-430-8574.

Acknowledgments
The authors thank Bo Jin for assistance in mouse husbandry.

CRediT Authorship Contributions
Winfried Edelmann, PhD (Conceptualization: Lead; Funding acquisition: Lead; Project administration: Equal; Writing – original draft: Lead; Writing – review and editing: Lead)
Elena Tosti, PhD (Conceptualization: Lead; Data curation: Lead; Formal analysis: Lead; Funding acquisition: Supporting; Investigation: Lead;

Methodology: Lead; Project administration: Equal; Visualization: Lead; Writing – original draft: Lead; Writing – review and editing: Lead)

Ana S. Almeida, PhD (Data curation: Supporting; Investigation: Supporting; Methodology: Supporting; Writing – review and editing: Supporting)

Tam T.T. Tran, PhD (Data curation: Supporting; Methodology: Equal; Software: Equal; Visualization: Equal; Writing – review and editing: Supporting)

Mariel Barbachan e Silva, MS (Data curation: Supporting; Methodology: Equal; Software: Equal; Visualization: Equal)

Pilib Ó Broin, PhD (Data curation: Supporting; Methodology: Equal; Software: Equal; Visualization: Equal)

Robert Dubin, PhD (Data curation: Supporting; Methodology: Equal; Software: Equal; Visualization: Supporting)

Andrew S Mclellan, PhD (Data curation: Supporting; Methodology: Supporting; Software: Equal; Visualization: Supporting)

Aaron Golden, PhD (Data curation: Supporting; Methodology: Supporting; Resources: Supporting; Writing – review and editing: Supporting)

Paul W O'Toole, PhD (Conceptualization: Supporting; Supervision: Supporting; Writing – review and editing: Supporting)

Amanda P Beck, DVM (Formal analysis: Equal; Methodology: Equal; Visualization: Equal; Writing – review and editing: Supporting)

Ken Chen, MD (Methodology: Supporting)

Eduardo Vilar-Sanchez, MD (Resources: Supporting; Writing – review and editing: Supporting)

Conflicts of Interest

The authors disclose no conflicts.

Funding

This work was supported by National Institutes of Health grants CA248536 and CA222358 (to Winfried Edelmann), a Feinberg Family Donation (to Winfried Edelmann and Eduardo Vilar-Sanchez), Cancer Center grant CA13330 (to Albert Einstein College of Medicine), and Department of Defense fellowship CA15080 (to Elena Tosti).